UNIVERZITA KARLOVA

Přírodovědecká fakulta

HABILITAČNÍ PRÁCE

Řízení aktivních míst v zeolitových katalyzátorech
(Engineering of active sites in zeolite catalysts)

Mariya Shamzhy

2022

Contents

Enclosures

Specific sections of this habilitation work annotate the following publications:

pp. 7-13

1. Opanasenko, **M. Shamzhy**, Y. Wang, W. Yan, P. Nachtigall, J. Čejka. Synthesis and post-synthesis transformation of germanosilicate zeolites. Angew. Chem. Int. Ed., 2020, 59, 19380–19389
   https://onlinelibrary.wiley.com/doi/full/10.1002/anie.202005776   **IF = 15.3**

2. **M. Shamzhy**, M. Opanasenko, F. S. de O. Ramos, L. Brabec, M. Horáček, M. Navaro-Rojas, R.E. Morris, H. Pastore, J. Čejka. Post-synthesis incorporation of Al into germanosilicate ITH zeolite: the influence of treatment conditions on acidic properties and catalytic behavior in tetrahydropyranylation reaction. Catal. Sci. Technol., 2015, 5, 2973–2984
   https://pubs.rsc.org/en/content/articlelanding/2015/cy/c4cy01594k#!divAbstract   **IF=6.1**

3. V. Kasneryk, M. Opanasenko, **M. Shamzhy**, Z. Musilová, Y. S Avadhut, M. Hartmann, J. Čejka. Consecutive interlayer disassembly-reassembly during alumination of UOV zeolite: insight into the mechanism. J. Mater. Chem. A, 2017, 5, 22576-22587 https://pubs.rsc.org/en/content/articlelanding/2017/ta/c7ta05935c#!divAbstract   **IF=11.3**

4. **M.V. Shamzhy***, P. Eliašová, D. Vitvarová, M. V. Opanasenko, D. S. Firth, R. E. Morris. Post-synthesis stabilization of germanosilicate zeolites ITH, IWW and UTL by substitution of Ge for Al. Chem. Eur. J., 2016, 22, 17377–17386
   https://chemistry-europe.onlinelibrary.wiley.com/doi/full/10.1002/chem.201603434   **IF=5.2**

5. **M. Shamzhy**, M. Opanasenko, Y. Tian, K. Konysheva, O. Shvets, P. Nachtigall, R. E. Morris, J. Čejka. Germanosilicate precursors of ADORable zeolites obtained by ITH, ITR and IWR zeolites disassembly. Chem. Mater., 2014, 26, 5789–5798
   https://pubs.acs.org/doi/10.1021/cm502953s   **IF=9.8**

6. V. Kasneryk**, M. Shamzhy**, M. Opanasenko, S. A. Morris, S. Russell, A. Mayoral, J. Čejka, R. E. Morris. Expansion of the ADOR strategy for the synthesis of new zeolites: The synthesis of IPC-12 from zeolite UOV. Angew. Chem. Int. Ed., 2017, 56, 324–4327. https://onlinelibrary.wiley.com/doi/10.1002/anie.201700590   **IF = 15.3**

7. **M. Shamzhy**, F. Solânea de O. Ramos, Tuning of acidic and catalytic properties of IWR zeolite by post-synthesis incorporation of three-valent elements. Catal. Tod., 2015, 243, 76–84
   https://www.sciencedirect.com/science/article/pii/S0920586114004829   **IF=6.7**

8. A. I Hussain, A. Palani, A. M Aitani, J. Čejka, **M. Shamzhy**, M. Kubů, S. S Al-Khattaf. Catalytic cracking of vacuum gasoil over-SVR, ITH, and MFI zeolites as FCC catalyst additives. Fuel Proces. Tech., 2017, 161, 23–32.
   https://www.sciencedirect.com/science/article/pii/S0378382016306890   **IF = 7.0**

9. J. Zhang, O. Veselý, Z. Tošner, M. Mazur, J. Čejka, M. Opanasenko and **M. Shamzhy***. Toward Controlling Disassembly Step within the ADOR Process for the Synthesis of Zeolites. Chem. Mater., 2021, 33, 1228 – 1237
   https://pubs.acs.org/doi/10.1021/acs.chemmater.0c03993   **IF=9.8**

10. J. Zhang, Q. Yue, M. Mazur, M. Opanasenko, **M. Shamzhy***, J. Čejka. Selective recovery and recycling of germanium for the design of sustainable zeolite catalysts. ACS Sust. Chem. & Eng., 2020, 345, 8235–8246
    https://pubs.acs.org/doi/10.1021/acssuschemeng.0c01336   **IF=8.1**

pp. 13-19

11. **M. Shamzhy**, B. Gil, M. Opanasenko, W. Roth, J. Čejka. MWW and MFI frameworks as model layered zeolites: structures, transformations, properties, and activity. ACS Catal., 2021, 11, 2366 – 2396

    https://pubs.acs.org/doi/10.1021/acscatal.0c05332 **IF = 13.0**

12. **M. Shamzhy***, J. Přech, J. Zhang, V. Ruaux, H. El-Siblani, S. Mintova. Quantification of Lewis acid sites in 3D and 2D TS-1 zeolites: FTIR spectroscopic study. Catal. Tod., 2020, 345, 80-87

    https://www.sciencedirect.com/science/article/pii/S0920586119305620 **IF=6.7**

13. I. Podolean, J. Zhang, **M. Shamzhy**, V.I. Parvulescu, J. Čejka. Solvent-free ketalization of polyols over germanosilicate zeolites: the role of the nature and strength of acid sites. Catal. Sci. Tech., 2020, 10, 8254 – 8264

    https://pubs.rsc.org/en/content/articlelanding/2020/cy/d0cy01662d#!divAbstract **IF=6.1**

14. Y. Zhou, S. A. Kadam, **M. Shamzhy***, J. Čejka, M. Opanasenko*. Isoreticular UTL-Derived Zeolites as Model Materials for Probing Pore Size-Activity Relationships. ACS Catal., 2019, 9, 5136–5146

    https://pubs.acs.org/doi/10.1021/acscatal.9b00950 **IF = 13.0**

15. T. Soták, Z. Magyarová, **M. Shamzhy**, M. Kubů, K. Gołąbek, J. Čejka, M. Hronec. Gas-phase etherification of cyclopentanol to cyclopentyl methyl ether catalyzed by zeolites. Appl. Catal. A, 2021, 618, 118122,

    https://doi.org/10.1016/j.apcata.2021.118122 **IF=5.7**

pp. 19-27

16. **M. Shamzhy**, M. Opanasenko, P. Concepción and A. Martínez, New trends in tailoring active sites in zeolite-based catalysts. Chem. Soc. Rev., 2019, 48, 1095-1149

    https://pubs.rsc.org/en/content/articlelanding/2019/cs/c8cs00887f#!divAbstract **IF=54.5**

17. M. Kubů, M. Opanasenko, **M. Shamzy**. Modification of textural and acidic properties of -SVR zeolite by desilication. Catal. Tod., 2014, 227, 15, 26-32 https://doi.org/10.1016/j.cattod.2013.11.063 **IF=6.7**

18. M. Alonso-Doncel, A. Peral, **M. Shamzhy**, J. Čejka, R. Sanz, D.P. Serrano. Untangling the role of the organosilane functional groups in the synthesis of hierarchical ZSM-5 zeolite by crystallization of silanized protozeolitic units. Catal. Tod., 2020, 345, 27-38 https://www.sciencedirect.com/science/article/pii/S0920586119306479 **IF=6.7**

19. M. Alonso-Doncel, A. Peral, **M. Shamzhy**, J. Čejka, R. Sanza, D.P. Serrano. Fine-tuning hierarchical ZSM-5 zeolite by controlled aggregation of protozeolitic units functionalized with tertiary amine-containing organosilane. Micropor. Mesopor. Mater., 2020, 303, 110189 https://www.sciencedirect.com/science/article/pii/S138718112030192X **IF=5.3**

20. S. Gutiérrez-Rubio, **M. Shamzhy**, J. Čejka, D.P. Serrano, I. Moreno, J.M. Coronado. Vapor phase acylation of guaiacol with acetic acid over micro, nano and hierarchical MFI and BEA zeolites. Appl. Catal. B, 2021, 285, 119826

    https://www.sciencedirect.com/science/article/pii/S0926337320312431 **IF = 19.5**

21. M. V. Opanasenko, **M.V. Shamzhy**, Ch. Jo, R. Ryoo, J. Čejka. Annulation of phenols: catalytic behavior of conventional and 2D zeolites. ChemCatChem, 2014, 6, 1919–1927 https://chemistry-europe.onlinelibrary.wiley.com/doi/full/10.1002/cctc.201402007 **IF=5.6**

22. P. Eliášová, M. Opanasenko, P. Wheatley, **M. Shamzhy**, M. Mazur, P. Nachtigall, W.J. Roth, R. E. Morris, J. Čejka. ADOR mechanism for the synthesis of new zeolites. Chem. Soc. Rev., 2015, 44, 7177–7206

    https://pubs.rsc.org/en/content/articlelanding/2015/cs/c5cs00045a#!divAbstract **IF=54.5**

23. M. Pitínová-Štekrová, P. Eliášová, T. Weissenberger, **M. Shamzhy**, Z. Musilová, J. Čejka. Highly selective synthesis of campholenic aldehyde over Ti-MWW catalysts by α-pinene oxide isomerization. Catal. Sci. Technol., 2018, 8, 4690-4701

    https://pubs.rsc.org/en/content/articlelanding/2018/cy/c8cy01231h#!divAbstract **IF=6.1**

24. M. Stekrova, M. Kubů, **M. Shamzhy**, Z. Musilova, J. Čejka. α-pinene oxide isomerization: Role of zeolite structure and acidity in selective synthesis of campholenic aldehyde. Catal. Sci. Technol., 2018, 8, 2488-2501

    https://pubs.rsc.org/en/content/articlelanding/2018/CY/C8CY00371H#!divAbstract **IF=6.1**

25. J.-Ch. Kim, R. Ryoo, M. V. Opanasenko, **M.V. Shamzhy**, J. Čejka. Mesoporous MFI Zeolite Nanosponge as a High Performance Catalyst in the Pechmann Condensation Reaction. ACS Catal., 2015, 5, 2596–2604

    https://pubs.acs.org/doi/10.1021/cs502021a **IF = 13.0**

26. S.A. Kadam, **M.V. Shamzhy***. IR Operando Study of Ethanol Dehydration over MFI Zeolite. Catal. Tod., 2018, 304, 51-57

    https://www.sciencedirect.com/science/article/pii/S0920586117306272 **IF=6.7**

27. S.A. Kadam, **M.V. Shamzhy**. IR Operando study of Ethanol Dehydration over MFI zeolites: Structure-Activity Relationships. J. Phys. Chem. C, 2018, 122, 24055-24067 https://pubs.acs.org/doi/abs/10.1021/acs.jpcc.8b05697 **IF=4.1**

pp. 27-33

28. W. Zhang, Y. Zhou, **M. Shamzhy**, S. Molitorisová, M. Opanasenko, A. Giroir-Fendler. Total oxidation of toluene and propane over supported Co3O4 catalysts: Effect of structure/acidity of MWW zeolite and cobalt loading. Appl. Mater. Interfaces, 2021, 13, 15143–15158 https://pubs.acs.org/doi/abs/10.1021/acsami.0c21999 **IF=9.2**

29. Y. Zhang, A. Li, M. Kubů, **M. Shamzhy***, J. Čejka. Highly selective reduction of biomass-derived furfural by tailoring the microenvironment of Rh@BEA catalysts. Catal. Tod., 2022, 390-391, 295-305.

    https://doi.org/10.1016/j.cattod.2021.09.031 **IF = 6.7**

30. Y. Zhang, K. Fulajtárová, M. Kubů, M. Mazur, **M. Shamzhy**, M. Hronec, J. Čejka. Controlling dispersion and accessibility of Pd nanoparticles via 2D-to-3D zeolite transformation for shape-selective catalysis: Pd@MWW case. Mater. Today Nano, 2019, 8, 100056 https://www.sciencedirect.com/science/article/pii/S2588842019301257 **IF=8.1**

31. S. Molitorisová, Y. Zhang, M. Kubů, A. Li, Z. Tošner, **M. Shamzhy***. 2D-to-3D zeolite transformation for the preparation of Pd@MWW catalysts with tuneable acidity. Catal. Tod., 2022, 390-391, 109-116

    https://www.sciencedirect.com/science/article/pii/S0920586121005241 **IF = 6.7**

32. Y. Zhang, A. Li, M. Sajad, K. Fulajtárová, M. Mazur, M. Kubů, **M. Shamzhy**, M. Hronec, R. Bulánek, J. Čejka. Imidazolium-type ionic liquid-assisted formation of the MFI zeolite loaded with metal nanoparticles for hydrogenation reactions. Chem. Eng. J., 2021, 412, 128599 https://www.sciencedirect.com/science/article/pii/S1385894721001972 **IF=13.2**

Outline

This habilitation work includes four chapters devoted to various aspects of the engineering of active sites in zeolite catalysts.

The first chapter systematizes our findings on the main factors controlling the isomorphous substitution of trivalent elements in the frameworks of germanosilicate zeolites and on the relationship between the chemical composition of new structural types of zeolites and their catalytic properties.

The use of FTIR spectroscopy to comprehensively characterize acid sites in zeolites is discussed further in the context of catalytic applications.

The third section presents our contribution to the accumulated knowledge on the synthesis-structure-performance relationships for zeolites with hierarchical porosity. The last section of this work discusses our recently developed synthetic approaches for atom-efficient synthesis of the metal-supported zeolites.

Engineering of Active Sites in Zeolite Catalysts

Introduction

Nowadays, more than 90 % of chemicals are manufactured in industry with the use of heterogeneous catalysts. About 130 of ~ 850 commercially available heterogeneous catalysts are based on zeolites, that is, crystalline microporous metallosilicates with three-dimensional frameworks. The principal building units of a zeolite are tetrahedra TO_4 (T = Si, B, Al, Ga, Ti, Sn, Ge, and others), which are connected *via* shared corners to form more complex secondary building units, constituting the framework. Elements with typical oxidation state +3, such as Al, Fe, Ga, impose a negative framework charge and give rise to Brønsted acidity, when compensated by a proton (Figure 1). After dehydroxylation, the Brønsted acid sites (BAS) may transform to Lewis acid centers (LAS). In turn, coordinatively unsaturated atoms of four-valent elements, such as Ti, Sn, Zr exhibit Lewis acidity (Figure 1), although BAS may be formed due to the coordination of water with the metal site.
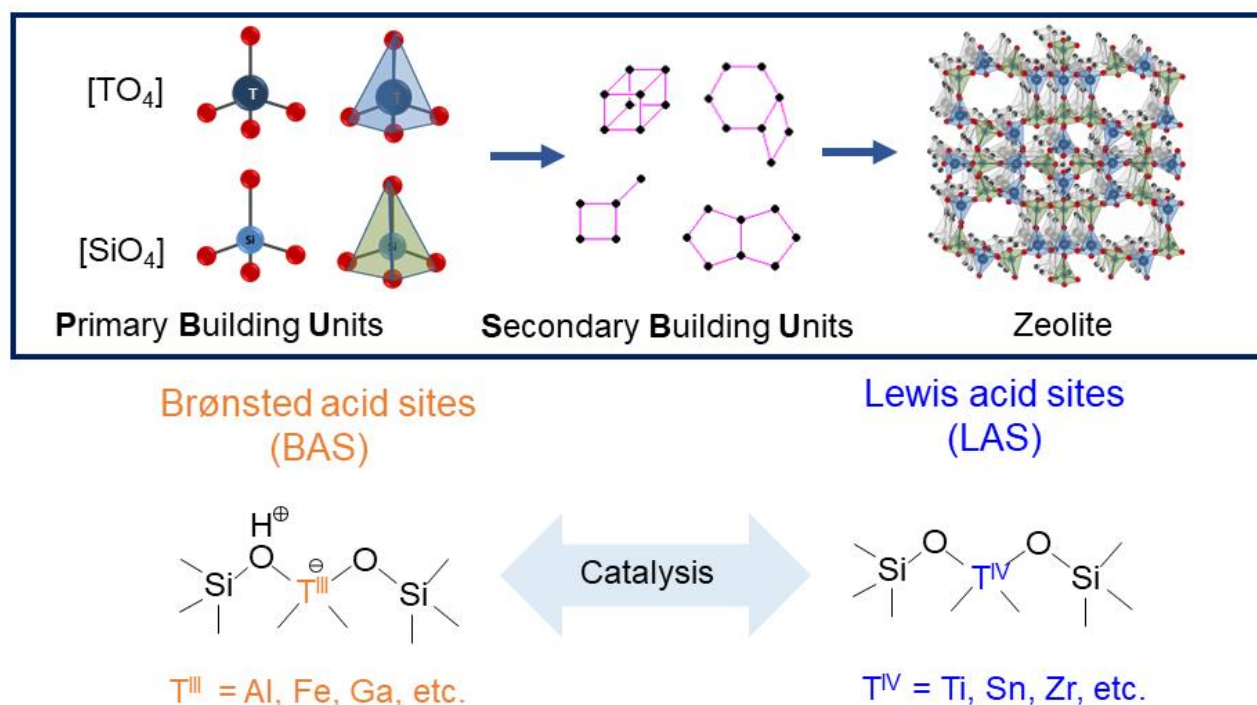

Figure 1. Schematic representation of (*top*) structure-building units of a zeolite framework and (*bottom*) different types of acid sites arising from isomorphous substitution in zeolites

Zeolite catalysts benefit from (i) a variable chemical composition providing tuneability of acid function; (ii) a uniform microporosity providing controllable product selectivity *via* molecular sieving effect; and (iii) a high thermal stability providing easy regeneration. Due to their acidic functionality, aluminosilicate zeolites are widely applied as industrial catalysts in

fluid catalytic cracking (FCC), transformation of methanol to hydrocarbons, petrochemical processes, such as alkylation and transalkylation, disproportionation and isomerization. **Due to a great plethora of possibilities for utilization of zeolites as tailor-made catalysts, the synthesis of novel topologies and modification of the properties of well-known zeolites are still the key targets**.

Over the past eight years, my research in zeolite chemistry was focused on the following aspects highlighted in this habilitation work:

- Tuning the nature of acid sites in zeolite catalysts;
- IR spectroscopic studies of zeolite catalysts;
- Acidity-performance relationships for hierarchical zeolite catalysts;
- Designing of metal-supported zeolite catalysts.

Tuning the nature of acid sites in zeolite catalysts

The last decade has brought about new types of zeolite-based materials that are outstanding candidates for the catalytic conversion of bulky molecules characteristic of fine chemistry. These materials include, in particular, zeolites with extra-large pores having diameters higher than 8.5 Å. Most extra-large pore zeolites were prepared as germanosilicates utilizing the tendency of Ge to direct the crystallization process toward low-framework density structures (*Angew. Chem. Int. Ed. 2020[1]*). Despite very promising results in catalytic tests on the laboratory scale, zeolites possessing extra-large channels and substituted with 3- and 4-valence elements have never reached wide-range applications. One of the reasons was low thermal and hydrolytic stability that restricted the utilization of germanium-containing zeolites at moderate to high temperatures. To extend the practical application of germanosilicate zeolites, we made use of the hydrolytic instability of Ge-O(Si) bonds for tuning the acid properties of the frameworks possessing Ge-rich double-four-ring (D4R) units propagated in one direction, such as ITH (*Catal. Sci. Tech. 2015*), UOV (*J. Mater. Chem. A 2017*), IWW and IWR (*Chem. Eur. J. 2016*). The lattice organization for the mentioned materials may be represented as dense Si-rich crystalline sheets alternated with Ge-rich D4R building units. The molar ratio of framework atoms (Si/Ge) in the starting solid determines the number of Ge−OSi links and thus affects the hydrolytic stability of germanosilicates. It was found that under specific conditions germanosilicates with high content of Ge (typical Si/Ge are in the range 6-to-8.5 depending on the zeolite structure) can undergo so-called framework disassembly by removal of Ge atoms, giving highly ordered materials composed of crystalline and relatively independent (not interconnected by covalent bonds) nanosheets. This provides the opportunity to perform different manipulations with the aim of modifying the organization of the layer's ensemble *via* changes in their mutual

---

orientation and in the structure of interlayer units (*Chem. Mater. 2014*). Successful application of this approach to UTL and UOV germanosilicates (*Angew. Chem. Int. Ed. 2017*) gave rise to at least seven new zeolite structures, none of which has yet been synthesized directly. The output of hydrolysis treatment depends on the presence of additional cations that may replenish the framework after the removal of Ge. If hydrolysis of germanosilicates such as ITH, UOV, IWW is performed in the acidic medium lacking framework-building elements (e.g., Al^{3+}), framework disassembly occurs. However, the same zeolites maintain their structural characteristics if acidic treatment is carried out in the presence of Al^{3+} cations. This result supported the involvement of Al cations in the healing of defects associated with various silanols, which are generated due to the breaking of the Ge–O(Si) linkages (Figure 2, *left*).
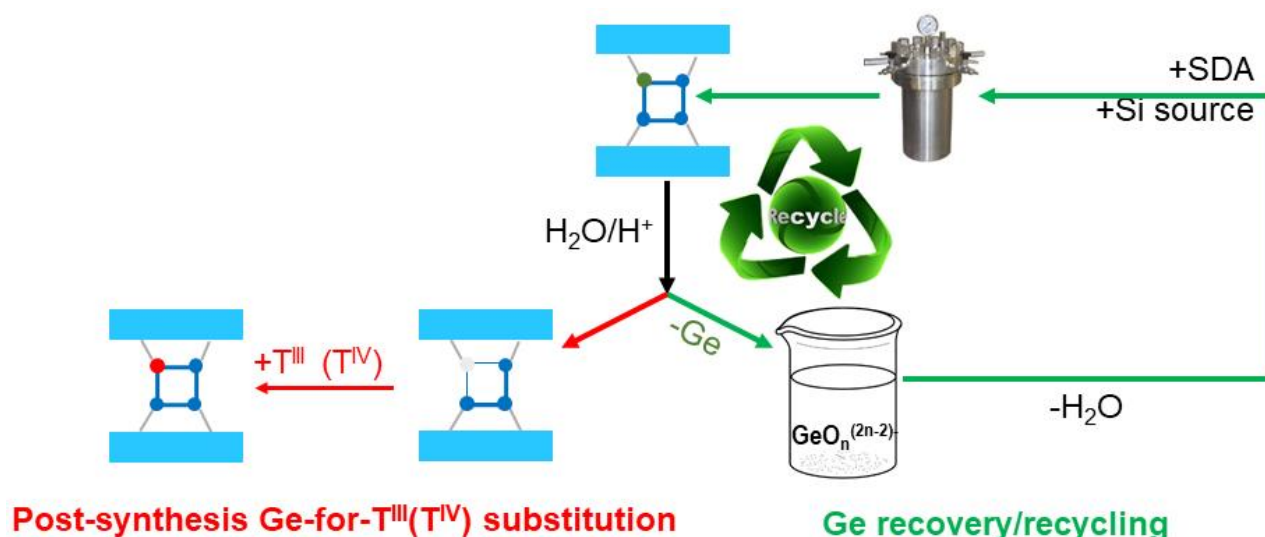

Figure 2. (*left branch*) Tailoring of variable acid sites *via* two-step post-synthesis isomorphous substitution of Ge (•) for the 3- or 4-valence element (•); (*right circle*) Recovery and recycling of extracted Ge. (•) represents silanol nest ($\equiv$Si-OH)$_4$ formed upon removal of a Ge atom from the framework

Al atoms incorporated into zeolite materials by this method were expected to give rise to Brønsted acid sites (BAS) for a range of catalytic applications. Thus, it was crucial to confirm the location of the atoms of Al in the zeolite framework (solid-state ^{27}Al NMR spectroscopy evidenced > 80 % of introduced Al atoms occupy tetrahedral framework positions) and to find ways to control their concentration. We found that both the properties of the starting materials (type of zeolite structure, crystal morphology, framework elements ratio, etc.) and the treatment parameters (temperature, time, pH, concentration of trivalent cation) influenced the total concentration of acid centers and, frequently, their distribution between Brønsted and Lewis types of centers. Independently of the type of the starting zeolite and its Si/Ge ratio, the most notable growth (50 – 150 %) in the concentration of BAS was detected with only a minor decrease in the concentration of the Lewis acid centers as the temperature of alumination increases from 80 to 175 °C. The critical role of temperature in the mentioned

range was related to more intensive facilitation of the condensation reaction (resulting in Si–O–Al framework linkages) compared to the removal of Ge from the zeolite lattice (breaking of Ge–O bonds similarly to the above-mentioned disassembly process) (*Catal. Tod. 2015*). We observed a drastic rise of the concentration for both BAS and LAS with decreasing crystal size of parent ITH germanosilicate, indicating diffusion control over post-synthesis isomorphous substitution. To maximize the concentration of Al-associated BAS upon post-synthesis Ge-for-Al substitution in zeolites, the treatment of germanosilicates using aluminum nitrate solutions with moderate acidity (pH = 2 is optimal in a pH range of 0.5 – 4) at elevated temperatures is recommended.

Simultaneously with enhancing the content of Al sites in post-synthetically aluminated ITH and IWW materials, a decrease in Ge concentration was observed. Generally, a drop in Ge content in materials with relatively high Si/Ge (> 6) usually corresponded to the concentration of incorporated Al, but remarkably exceeded the amount of Al included in germanosilicate zeolites with lower Si/Ge (< 6). This inequivalent substitution of Ge for Al allowed us to vary the porous system of Ge-enriched zeolites. As an example, the incorporation of Al in zeolites of ITH, UOV, and IWW topologies with high Ge content resulted in the generation of relatively large pores with diameters exceeding 2 nm (mesopores). Thus, the treatment led to stabilized (in terms of hydrolytic and thermal stability) zeolites with classical chemical composition (Si and Al) and hierarchical pore system containing both micropores and mesopores. In particular, exchange of Ge to Al by post-synthetic modification of Ge-rich ITH possessing micropores of medium size generated strong protonic acid centers with higher accessibility for large-sized molecules like 2,6-di-*tert*-butyl pyridine (confirmed by FTIR spectroscopy) if to compare with the reference aluminum-containing ITH zeolite obtained by direct synthesis.

Contrary to the treatments aimed at the incorporation of Al or Ga, disassembly (hydrolysis of chemically labile Ge–O links) was shown to dominate when Fe^{3+} was selected as an element for introduction into the zeolite lattice. This was explained by the relatively high ionic radius of iron ions compared to aluminum, as well as the increased tendency of Fe^{3+} ions to possess octahedral coordination, hindering the integration of cations into lattice vacancies (*Catal. Tod. 2015*).

Thus, the developed methods for incorporation of 3-valent elements allowed us not only to improve hydrolytic stability and to generate acid centers of different strengths, but also to modify the textural properties of germanosilicates. Strong acidity and developed mesoporosity in 3-valent element-substituted germanosilicates were reflected in their catalytic properties:

-in tetrahydropyranylation of alcohols, the yield of targeted alkyl-tetrahydropyranyl ethers was found to increase with growth in <u>acid centers strength </u>(i.e., in the order B- < Ga- < Al-substituted zeolites) or with
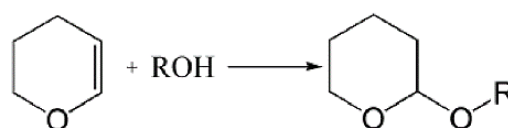
increasing the <u>concentration of accessible acid centers</u> (i.e., hierarchical micro-mesoporous Al-substituted germanosilicates performed better in comparison with microporous Al-containing zeolites synthesized directly). The latter tendency was more pronounced with increasing the size of alcohol reactant molecules studied (CH_3OH (3.6 Å) < C_3H_7OH (4.7 Å) < $C_6H_{13}OH$ (6.2 Å)).

-in acylation of p-xylene with benzoyl chloride, the activity of isomorphously substituted germanosilicates increased with the <u>number of accessible acid centers.</u> The higher strength of the gallium sites in comparison to the boron ones allowed efficient conversion of reacting molecules over Ga-IWR, while relatively low adsorption affinity of the Ga sites in comparison to stronger Al acid centers toward the reaction product conditioned higher yield over Ga-IWR. Thus, the catalyst activity increased in the order B-IWR << Al-IWR < Ga-IWR.
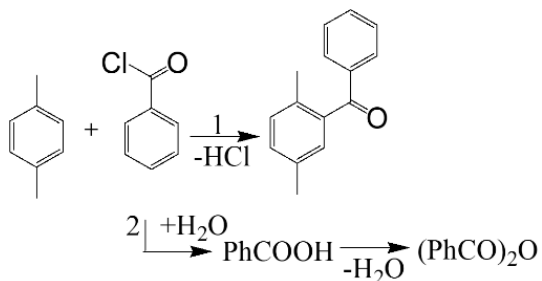
-Post-synthetically aluminated medium-pore ITH zeolite was found to be a promising additive to the FCC catalyst, enhancing the propylene yield twice compared to an equilibrium FCC catalyst (*Fuel Proces. Tech. 2017*).

Aiming to improve the application prospects of designed catalysts, we showed the possibility to recover costly Ge (*ACS Sust. Chem. Eng. 2020*) after its extraction from a zeolite framework (Figure 2, *right*). The extraction step releasing up to 94 % of Ge from IWW framework into the leaching solution was followed by separation of the parent zeolite *via filtration* using a qualitative filter paper (grade 601) or *microfiltration* using a membrane filter with pore size of 0.025 μm. After evaporation of the leaching solution, two forms of GeO_2 were obtained (Figure 3). The XRD patterns of both recovered samples corresponded to commercial GeO_2, while their IR spectra displayed bands of silicon-oxygen vibrations, which might indicate the presence of residual zeolite species. This assumption was verified by the transmission electron microscopy (TEM) study, which showed that large IWW zeolite particles remained in the leaching solution after filtration, while microfiltration allowed us to remove those particles (Figure 3). These remained particles served as seeds directing the crystallization process toward the formation of initial IWW zeolite independently of synthesis conditions and the type of the organic structure-directing agent (SDA) used. In contrast, microfiltration allowed us to recover zeolite-seed-free GeO_2, confirmed to be an appropriate form of Ge for the preparation of various germanosilicates (Figure 3).

Contrary to other Ge-containing zeolites possessing chemically labile D4Rs located between hydrolytically stable two-dimensional units, adding Al upon acidic treatment in aqueous medium did not lead to stabilization of extra-large pore UTL zeolite. It was related
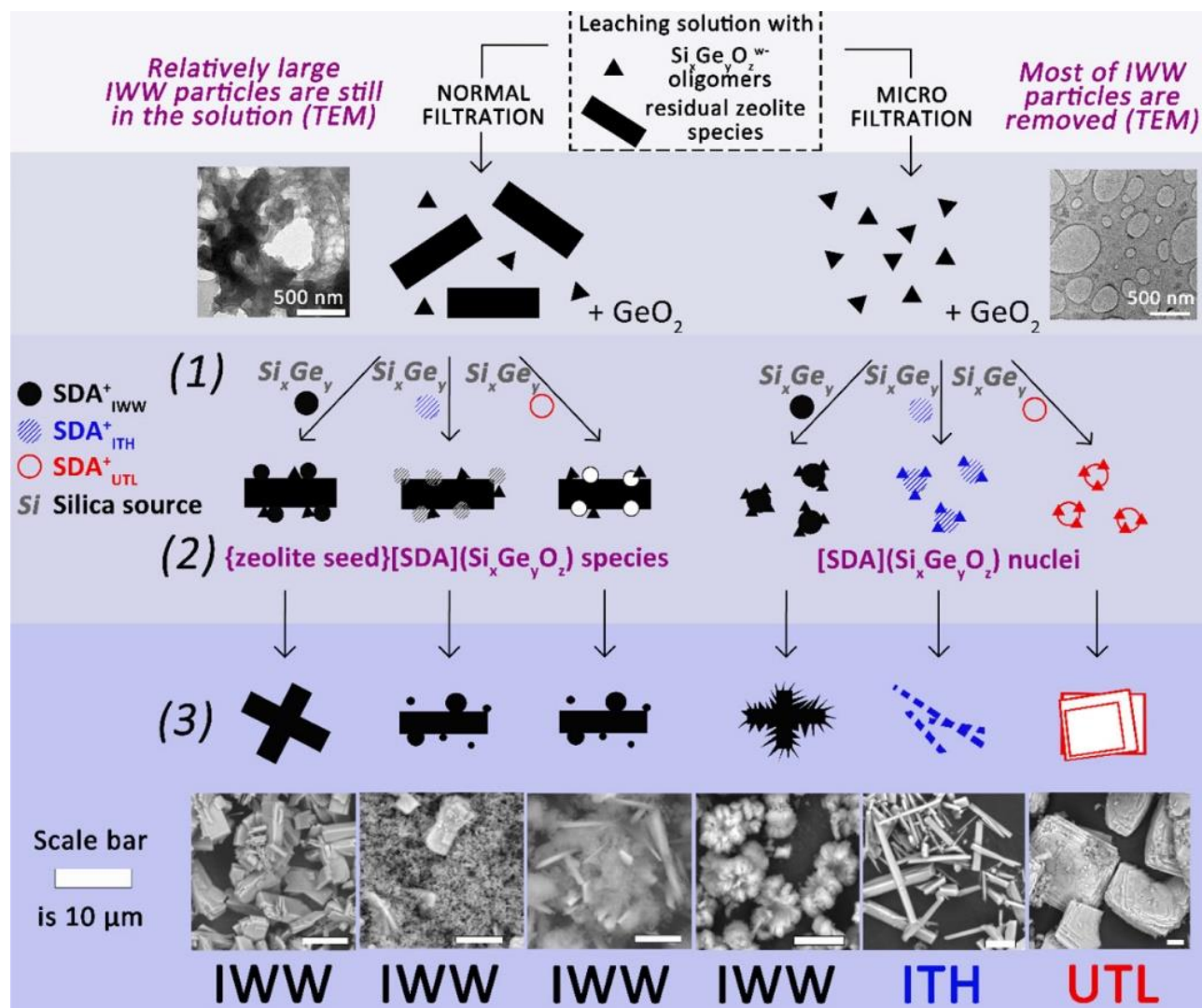
Figure 3. Schematic representation of the zeolite crystallization pathways depending on the morphological properties of GeO$_2$ as a source of Ge recovered by filtration (*left branch*) or microfiltration (*right branch*). Reprinted from *ACS Sust. Chem. Eng. 2020*

to the fast deintercalation of Ge-enriched species out of the UTL lattice and interlayer space, causing the rapid formation of layered IPC-1P material. To slow down the de-intercalation process, we used a mixed water/methanol solution as the medium for UTL hydrolysis (*Chem. Mater. 2021*). To promote the rearrangement process and generate strong acid sites, the source of Al was added. The evolution of interlayer d-spacing in the products of UTL transformation in Al-free and Al-containing water-methanol medium was analyzed using X-ray diffraction (XRD). We found that unlike water solutions, where leaching and further elimination of Ge atoms from the space between zeolitic nanosheets is fast, disassembly was slowed-down with decreasing H$_2$O in water-methanol systems. The results of the XRD analysis revealed a sequential size reduction of D4R units in water-methanol solution, that is, the transformation of D4R → D4R/S4R → S4R → S4R/oxygen bridges → oxygen bridges

with the formation of phase pure IPC-n zeolites after certain times (Figure 4, *top, left*). Unprecedentedly, further addition of Al as the source of framework-building element allowed us to reconstruct the original D4R interlayer links under slow disassembly conditions after 60 days of the treatment (Figure 4, *top, right*). The sequential transformation of D4R units in UTL zeolite was manifested not only by the interlayer d-spacing change, but also by the change in volume and size of the zeolite channels, which decreased upon conversion of D4R-into-S4R units and then restored upon S4R-to-D4R reconstruction. TEM images
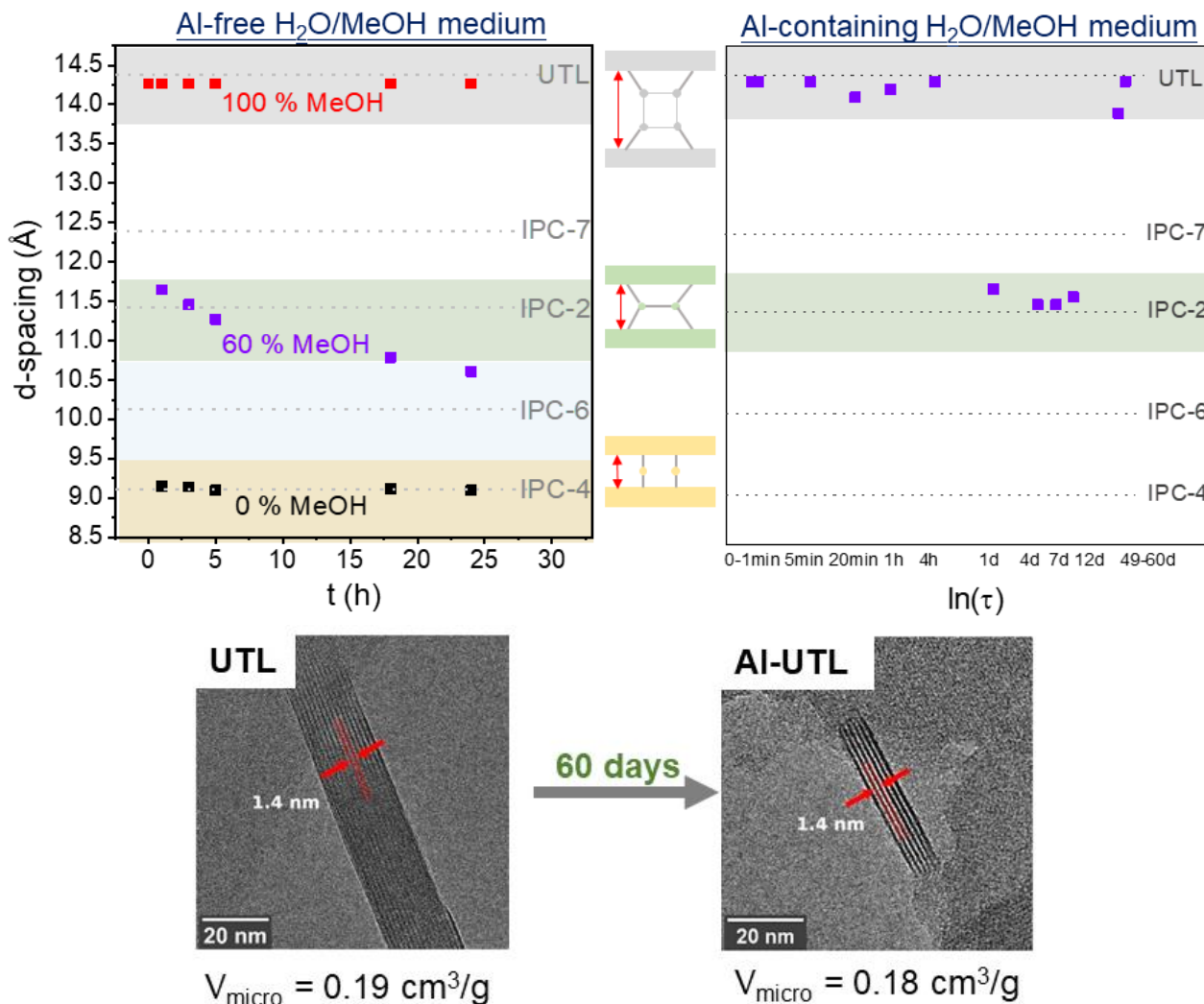
Figure 4. (*top*) Time-dependent change of (200) d-spacing (reflects the change in interlayer distance) in calcined samples obtained from UTL in water–methanol medium with different alcohol content in Al-free (*left*) and Al-containing systems (*right*). (*bottom*) TEM images of the initial and Al-substituted zeolite obtained by the treatment of UTL in Al-containing water–methanol medium and further calcined. Reprinted from *Chem. Mater. 2021*

showed stacked layers with 1.4 nm repeat for both the restored and parent UTL (Figure 4, *bottom*). Chemical analysis showed a gradually decreased amount of Ge in the zeolite along with increased Al content. Solid-state ^{27}Al NMR spectra revealed gradual insertion of aluminum in the zeolite lattice because the ratio of framework/extra-framework Al progressively increased and then remained unchanged. As a final point, the Al-assisted transformation of germanosilicate UTL to aluminosilicate with the same topology provided a high concentration of protonic and coordinatively unsaturated strong acid sites (0.2 – 0.3 mmol/g), known as active centers in various acid-catalyzed reactions.

Overall, the comprehensive characterization data allowed us to propose a possible mechanism of sequential transformation of UTL zeolite in Al-containing water-methanol medium (Figure 5):

- *1min-1h*: slow breaking of Ge–O bonds leading to slight structural disorder of the initial zeolite lattice and partial blockage of micropores with removed Ge-containing debris;
- *1h-1d*: de-intercalation of non-framework Ge species and insertion of extra-framework Al into the interlayer space, which led to formation of IPC-2 (OKO) zeolite with low Al content and poor crystallinity;
- *1-12days*: Al incorporation accompanied by self-organization of zeolitic nanosheets results in the material with the same topology (OKO), but significantly improved structural ordering and with major fraction of aluminum located in tetrahedral positions in the lattice;
- *12-60days*: continuation of aluminum incorporation at inhibited de-intercalation leads to the full restoration of structural units typical for initial zeolite.
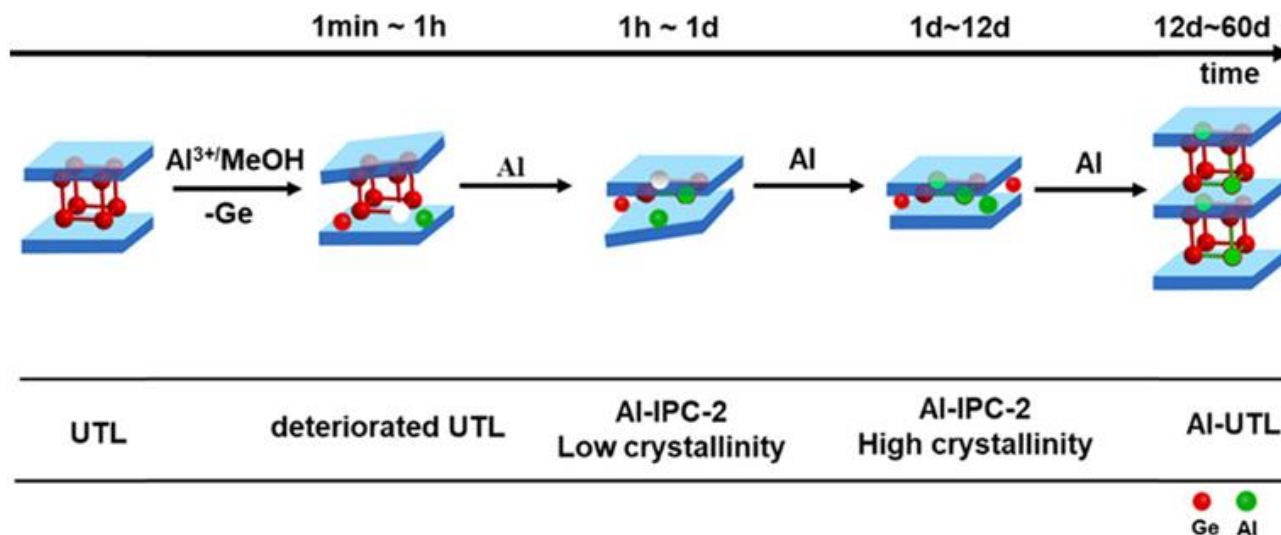

Figure 5. Possible mechanism for Al-assisted sequential structural changes of UTL germanosilicate in Al-containing water–methanol medium. Reprinted from *Chem. Mater. 2021*

The presence of small structural units characteristic of germanosilicate zeolites results in low densities and high pore volumes of these materials, which makes them appropriate for catalytic conversion of bulky molecules. Yet, their weak acidity and low hydrothermal stability along with high cost limited application of Ge-containing zeolites. Within presented studies, the methods for incorporation of different 3-valent elements into the framework of germanosilicate zeolites were developed and successfully applied to ITH, UOV, IWW, IWR and UTL germanosilicates. The basic factors controlling the isomorphous substitution of Ge in zeolites were generalized. The catalytic performance of novel materials was investigated in some important acid-catalyzed reactions and related to their textural and acidic properties being tuned by variation of the synthesis conditions. The developed methods for post-synthesis isomorphous substitution of Ge provides the way for tuning the active sites in zeolite catalysts with the micropore entrances larger than 12-ring, thus solving one of the long-standing challenges in zeolite catalysts design.

IR spectroscopic studies of zeolite catalysts

FTIR spectroscopy is one of the powerful tools for measuring zeolite acidity. In contrast to titration, thermal analysis, and calorimetry, FTIR not only provides information about the concentration of acid centers, but also allows differentiating their nature (i.e., Lewis and Brønsted). A detailed study of the strength, location, nature, and concentration of acid centers in zeolites is usually realized by adsorption of probe molecules monitored with FTIR spectroscopy (*ACS Catal. 2021*). d_3-acetonitrile (proton affinity is 783 kJ/mol) and pyridine (proton affinity is 912 kJ/mol) are among the most accepted basic probe molecules used for this purpose. Pyridine was first proposed as a probe molecule for solid acids in 1963 (*E.P. Parry, J. Catal., 1963, 2, 371*). Specific bands, arising from the interaction of pyridine with acid centers of different nature in the 1600 - 1400 cm^{-1} region, allow distinguishing Lewis and Brønsted acid sites. With Lewis acid sites pyridine forms a coordinative bond. On the contrary, pyridine is protonated by strong BAS. These interactions give rise to bands at 1445–1462 cm^{-1} and 1544 cm^{-1} assigned to pyridine that interacts with LAS (Figure 6, *left*) and pyridinium ions, respectively. Temperature-programmed desorption of pyridine (as well as of smaller strong base ammonia) monitored with FTIR spectroscopy is used to study the strength of acid sites. In turn, to identify the location of acidic sites within the channels or on the outer surface of a zeolite, alkyl-substituted pyridines are used, such as pyridine (≈ 6 Å, entering 10-ring but not 8-ring pores), 2,6-dimethylpyridine (≈ 7 Å), 2,4,6-trimethylpyridine (7–8 Å, entering 12-ring pores). In contrast, for the quantitative characterization of centers located in relatively narrow pores (<10-ring), less bulky ammonia or deuterated acetonitrile are preferred probes. When d_3-acetonitrile interacts with acid centers of zeolite, the C≡N stretching vibration band (2265 cm^{-1}) is red-shifted depending on the intrinsic properties of the acid centers. A band at 2297 cm^{-1} was attributed to the nitrile group interacting with BAS in aluminosilicates. Two types of aluminum centers (bands at 2325 and 2315 cm^{-1}) can be

distinguished using the signals at higher frequencies corresponding to different modes of C≡N group interactions with Lewis-type acid centers (*S. Bordiga et al, Chem. Soc. Rev., 2015, 44, 7262*).
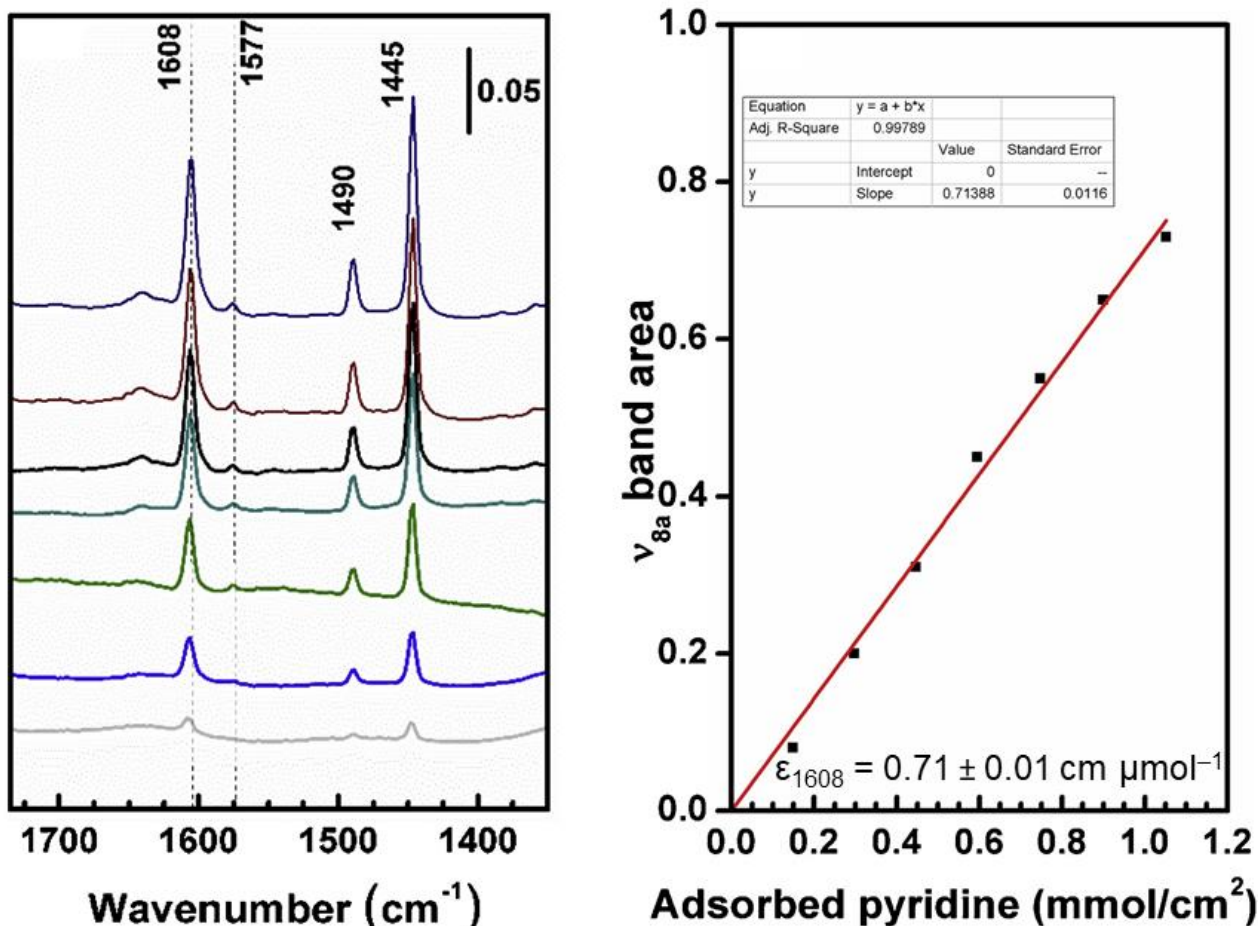

Figure 6. (*left*) IR spectra of titanosilicate MFI zeolite at increasing dosing of pyridine. (right) Integral intensity of the band at 1608 cm^{-1} versus the amount of pyridine adsorbed in titanosilicate MFI. Reprinted from *Catal. Tod.* 2020

Estimation of the acid site number in zeolites with variable chemical composition is challenging due to the necessity for determining the specific molar absorption coefficient. For that reason, only qualitative characterization of acid sites in titanosilicate zeolite catalysts was available for a long time. In our work (*Catal. Tod.* 2020), we developed an approach for evaluation of the Lewis acid centers in titanosilicates using FTIR spectroscopy of adsorbed pyridine. Unlike aluminosilicate zeolites, Lewis acid centers in titanosilicates were found to be of a low strength, which precluded the application of conventional method for their quantification (that is, tracing the intensity of the band at 1445 cm^{-1}). As an alternative, we have shown that the pyridine adsorption/desorption data at 50 °C, in particular the

normalized peak area related to the band at 1608 cm^{-1}, can be used to quantify the total amount of Lewis centers in titanosilicate catalysts with MFI topology. To determine the molar absorption coefficient ε, we used the volumetric method and estimate ε_{1608}(Ti Lewis site) value as 0.71 ± 0.01 cm μmol^{-1} (Figure 6).

FTIR spectroscopic study allowed us to understand the active sites responsible for glycerol ketalization to solketal over germanosilicate zeolite IWW (*Catal. Sci. Tech. 2020*). An interesting finding was an increasing conversion of glycerol over IWW germanosilicate with a decreasing activation temperature. To investigate the correlation between acidic features of IWW zeolite and activation conditions in more detail, we characterized the type, number, and strength of acid centers in the catalyst activated at different temperatures using FTIR spectroscopy and pyridine probe (Figure 7, *left*).
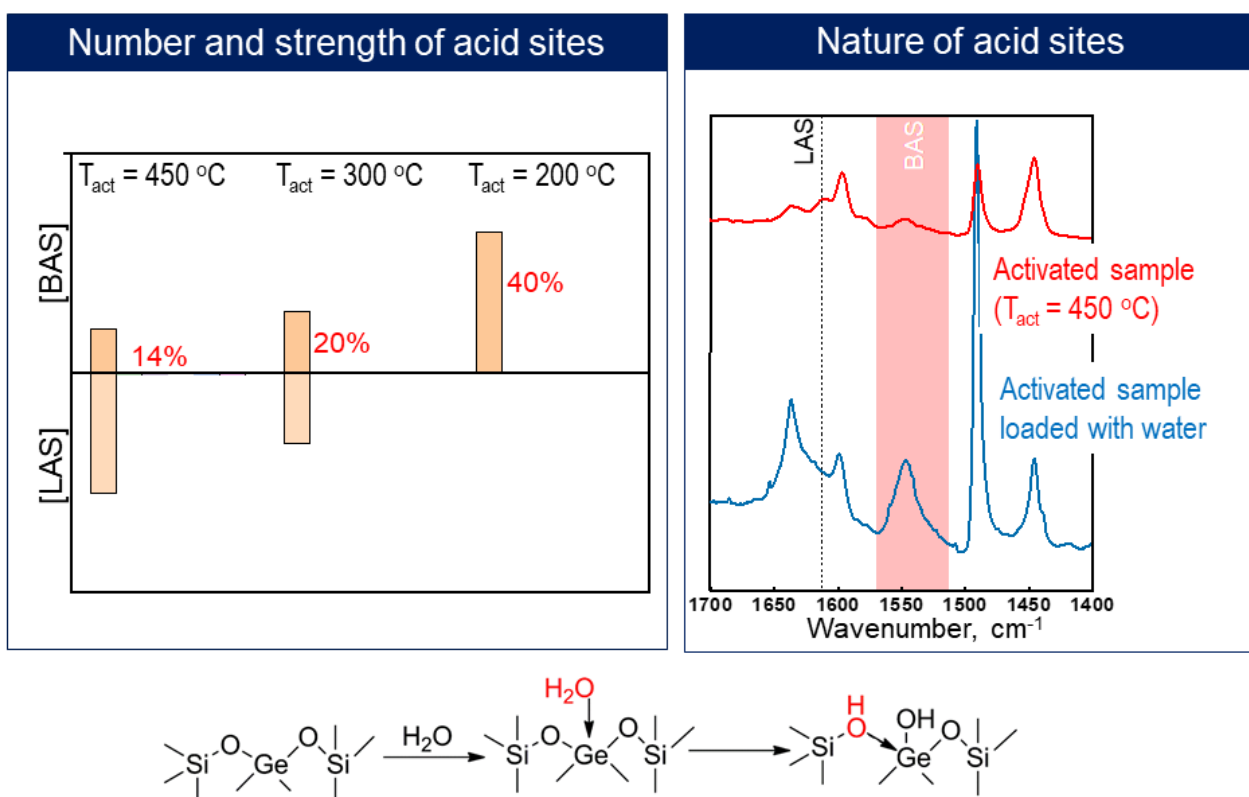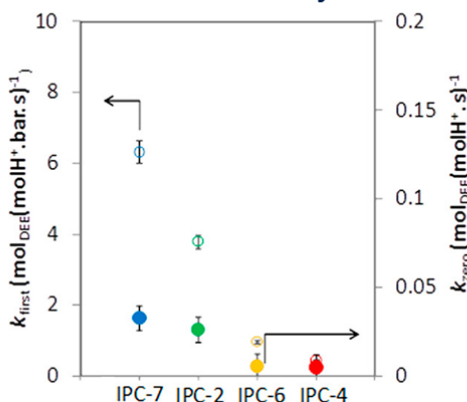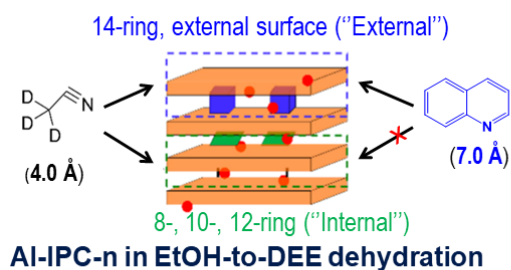

Figure 7. (*left*) Number of Brønsted acid sites (BAS) and Lewis acid sites (LAS) in IWW germanosilicate depending on the activation temperature. The fraction of "medium-strength" BAS not releasing pyridine at 100 $^{\circ}$C are shown as red numbers. (*right*) FTIR spectra of pyridine adsorbed in IWW zeolite activated at 450 $^{\circ}$C or in IWW zeolite activated at 450 $^{\circ}$C and subsequently loaded with water. Water-induced formation of BAS in IWW germanosilicate. Reprinted from *Catal. Sci. Tech. 2020*

The intensities of the characteristic absorption bands at 1545 and 1608 cm^{-1} were evaluated to estimate the concentrations of Brønsted and Lewis acid centers, while thermodesorption results allowed the distinction of the strength of acid sites. We found that decreasing activation temperature resulted in enhancing the strength of the BAS and increasing their

relative concentration at the expense of the LAS. Noticeably, the adsorption of water on the activated zeolite changed the distribution of acid sites in the IWW zeolite in a similar way (Figure 7, *right*). The obtained results were rationalized by assuming the formation of weak Brønsted acid centers upon the polarization of water molecules coordinated with LAS in IWW zeolites. The catalytic results reveal a higher activity of thus formed Brønsted acid sites in the ketalization reaction if one compares it with the Lewis acid centers.

FTIR spectroscopic study using probe molecules of different sizes supplemented our research on the pore size – activity relationships for "isoreticular" Al-IPC-n zeolites (n = 2, 4, 6, 7, Figure 8), that is, zeolites with the same topology of the layers but changed interlayer connectivity (*ACS Catal. 2019*). The distribution of acid centers between channels of different size was studied using d_3-acetonitrile (kinetic diameter 4.0 Å) and quinoline (7.0 Å) as probes. As illustrated in Figure 8, all acid sites in "isoreticular" zeolites are accessible to d_3-

FTIR spectroscopic study on the distribution of acid sites in isoreticular zeoltes

14-ring, external surface ("External")

(4.0 Å)   (7.0 Å)

8-, 10-, 12-ring ("Internal")

Al-IPC-n in EtOH-to-DEE dehydration

Zeolite	Channel dimension			Acid sites, mmol/g	External acidity	Internal acidity
Al-UTL	14 X 12 -ring					
Al-IPC-7	14 X 12 -ring	12 X 10 -ring		0.39	35 %	65 %
Al-IPC-2		12 X 10 -ring		0.37	29 %	71 %
Al-IPC-6		12 X 10 -ring	10 X 8 -ring	0.37	25 %	75 %
Al-IPC-4			10 X 8 -ring	0.40	21 %	79 %

Figure 8. Probe molecules used for FTIR spectroscopic study of the acid sites (shown as red dots) distribution in Al-IPC-n zeolite catalysts. Zeroth order and first-order rate constants of Ethanol-to-DEE dehydration on Al-IPC-n zeolite catalysts. Reprinted from *ACS Catal. 2019*

acetonitrile. In contrast, larger quinoline molecules could access only sites in 14-ring pores and on the external surface. Therefore, using d_3-acetonitrile adsorption, we found a similar total concentration of acid centers in Al-IPC materials at approximately 0.4 mmol/g, while using co-adsorption of quinoline and deuterated acetonitrile, we validated the highest fraction of more accessible acid centers in Al-IPC-7 zeolite featuring the largest pores. After the

acidic characteristics of "isoreticular" zeolites were assessed, we studied their activity in ethanol-to-DEE dehydration model reaction. For all "isoreticular" zeolites, the measured turnover rates for ethanol-to-DEE dehydration corresponded to the first-order kinetics at P_{EtOH} < 24 mbar and the zeroth-order kinetics at P_{EtOH} > 24 mbar. Related rate constants for first order (k_{first}) and zeroth order (k_{zero}) reactions were extracted using nonlinear regression of rate equation expressed by the associative dehydration mechanism observed over different acid catalysts (*R.T. Carr et al, J. Catal., 2011, 278, 78; A.J. Jones, J. Phys. Chem. C, 2014, 118, 17787; J.R. Di Iorio, ACS Catal., 2017, 7 (10), 6663*). Although k_{zero} was shown to primarily depend on the acid site strength, k_{first} is influenced by both the confinement and strength of the acid sites. In line with the similar strength of the acid centers in "isoreticular" zeolites, the values of k_{zero} had similar values (Figure 8). At the same time, expectedly higher values of the k_{first} constants for Al-IPC-2 and especially Al-IPC-7 zeolites (Figure 8) were consistent with better stabilization of the bulky ethanol dimeric transition state in larger pores of those zeolites. Because these findings match the expected results from the predictive analysis for the correlation of site location and apparent kinetics, they confirm the high potential of Al−IPC-n zeolites as model catalytic materials for assessing confinement−activity relationships to optimize relevant Brønsted acid-catalyzed reactions.

For MFI zeolite-catalyzed cross-etherification involving cyclopentanol and methanol, the reaction pathway was verified using a subsequent adsorption of both reactants examined with FTIR spectroscopy (*Appl. Catal. A 2021*). FTIR-monitored adsorption of cyclopentanol on a zeolite containing pre-adsorbed methanol revealed a gradual exchange of surface methanol molecules by those of cyclopentanol, as evidenced by the continual decrease in the intensity of the 2957 cm^{-1} band (characteristic of methanol, Figure 9, *top*) and the bands at 2970 cm^{-1} and 2883 cm^{-1} (characteristic of cyclopentanol). On the contrary, the zeolite sample pre-loaded with cyclopentanol did not adsorb methanol. The FTIR results were in line with the Riedel-Eley mechanism of cyclopentylmethyl ether formation over MFI zeolite (Figure 9, *bottom*). The first step of the reaction path is the hydrogen bonding of cyclopentanol molecules with Brønsted acid centers. The following step includes the attack of the methanol molecule on the C-atom of hydrogen-bonded species formed on the first step. As a result, a new C−O linkage of unsymmetrical ether is formed. The last step includes the desorption of water and cyclopentyl methyl ether molecules from Brønsted acid centers.

FTIR spectroscopy of adsorbed probe molecules, considered a well-established technique for the qualitative and quantitative analysis of the acidic characteristics of aluminosilicate zeolites, has so far been undeservedly underused for germanosilicate and titanosilicate zeolites. In our work we have shown that FTIR spectroscopy of adsorbed pyridine is suitable for assessing weak Ti- and Ge-associated Lewis acid sites. At the same time, it was shown that vibrational spectroscopy can contribute notably not only to the elucidation of the acid site characteristics in zeolite catalysts but also to the understanding of some steps of the catalytic reaction mechanism when reactants are used as probe molecules.
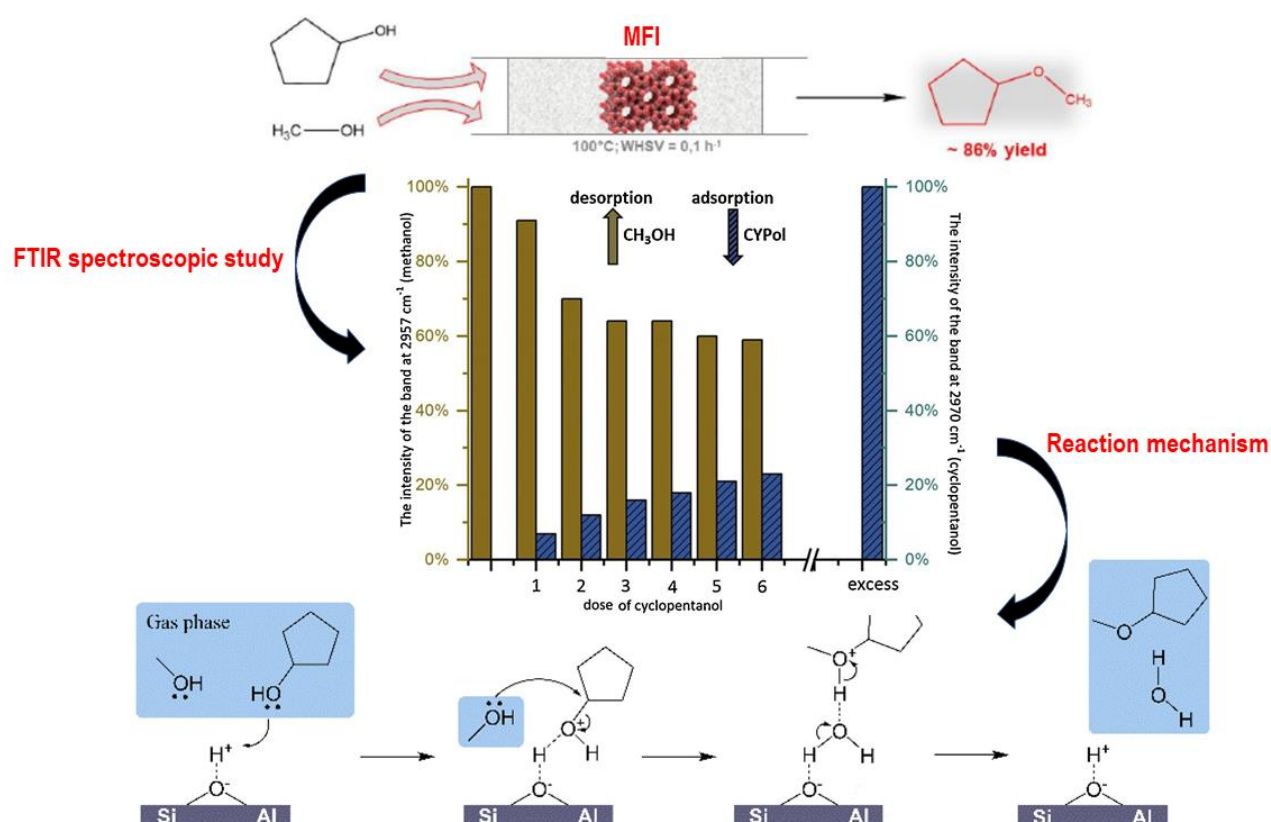
Figure 9. (*top*) Evolution of methanol (brown) and cyclopentanol (blue) band intensity in FTIR spectra of MFI zeolite pre-loaded with methanol and subjected to dose-by-dose injections of cyclopentanol; (*bottom*) Riedel−Eley mechanisms of cyclopentanol cross-etherification with methanol on MFI zeolite catalyst. Reprinted from *Appl. Catal. A 2021*

Acidity-performance relationships for hierarchical zeolite catalysts

The reduction of mass transfer limitations in the zeolite pore system is a prominent concept to enhance the performance of zeolite catalysts, which was developing over the last decade (Figure 10).

Hierarchical zeolites with intra-crystalline mesoporosity have been prepared either by post-synthesis elimination of a fraction of lattice atoms (V. *Valtchev et al, Chem. Soc. Rev, 2013, 42, 263*) or *via* direct routes using soft (surfactants, polymers) or rigid (e.g., carbon nanostructures) structure-directing agents (*Chem. Soc. Rev. 2019*). Although demetallation (Figure 10, *top*) is a more cost-efficient method for engineering mesoporosity in zeolites, this synthetic approach lacks control over the diameter of formed pores as well as over the number of active centers, thus preventing the tailor-made design of the catalysts (*Catal. Today 2014*).
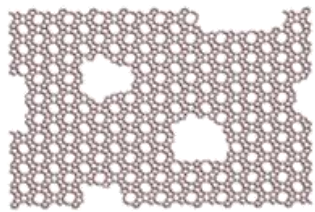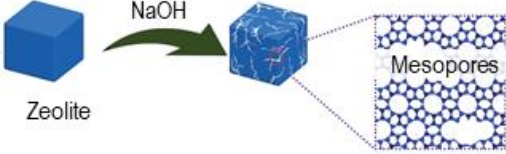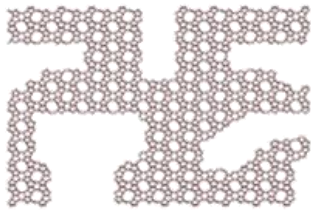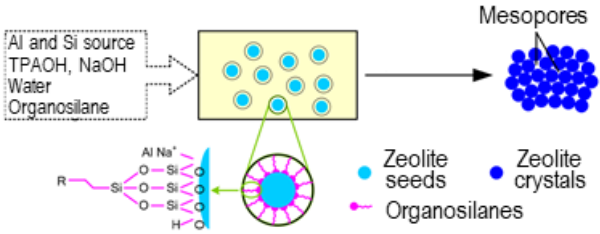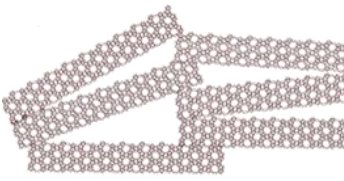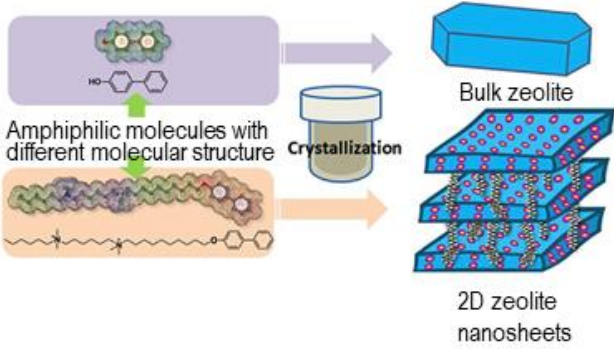
	Schematic representation	Synthetic strategy used
Hierarchical zeolites		**Demetallation** (D. Wang et al, J. Mater. Chem. A, 2015, 3, 3511)
Nanocrystalline zeolites		**Organosilane-assisted crystallization** (D. Wen et al, Ind. Eng. Chem. Res., 2018, 57, 446)
Layered (2D) zeolites		**Amphiphilic SDA-assisted crystallization** (X. Yan et al, Micropor. Mesopor. Mater., 2019, 279, 278)

Figure 10. Zeolites with enhanced accessibility of active sites: material types with synthetic strategies for their preparation

Zeolite nanocrystals with prominent intercrystalline mesoporosity were synthesized using various **organosilanes** as crystal-growth modifiers (*S. Mintova et al, Chem. Soc. Rev, 2015, 44, 7207)*. This approach uses chemical similarity of the modifier and the inorganic species, which form the zeolite framework (Figure 10, *middle*). Bulky organosilanes strongly interact with growing crystal domains of relatively small size and suppress the further propagation of crystal growth (*Catal. Today 2020*). The removal of organics at elevated temperature results in a hierarchical zeolite possessing the additional porosity associated with the interparticle

void volume previously occupied by organic groups of the organosilane modifier. We have first shown that the use of commercially available DEAMP organosilane ((Et$_2$N)C$_3$H$_6$[Si(OMe)$_3$]) containing tertiary amino group results in nanocrystalline MFI that is characterized not only by a remarkably high external surface (230 – 400 m^2/g), but also by a uniform transport pore size distribution (mesopore mean diameter centered at 4 nm) when comparing with previously reported materials obtained using more basic silanization agents containing primary or secondary amine groups (*Micropor. Mesopor. Mater. 2020*). An increase in the content of the organosilane in the synthesis gel from 2.5 to 10 mol.% (related to the total amount of Si) resulted in a progressive increase in the mesopore/external surface areas of the hierarchical zeolites formed. The activity of thus prepared nanocrystalline *vs.* conventional MFI demonstrated in the cracking of polyolefins was found to be dependent not only on the external surface, but also on BAS/LAS ratio (Figure 11, *left*), which are tunable by the variation of the amount of organosilane modifier added to the mixture upon zeolite synthesis. Nanocrystalline MFI zeolite obtained with 5 mol.% DEAMP (NZ$_{5.0}$ in Figure 11) and exhibiting relatively high concentration of BAS showed maximal conversion, while a significant decrease in activity was observed for zeolites prepared with lower (2.5 mol. %) or higher (7.5 – 10 mol. %) amounts of DEAMP. The result is explained by the opposite effect of DEAMP concentration on the values of the external/mesopore surface area and the BAS/LAS ratio. Noticeably, hierarchical zeolites with highly accessible acid sites were more active than conventional MFI zeolite in catalyzing the transformation of small-chain alkenes to larger-size products, thus showing higher selectivity toward liquid hydrocarbons (C5 – C12 selectivity in Figure 11).

By analyzing the performance of nanocrystalline and conventional zeolites with MFI structure as catalysts in acylation of biomass-derived guaiacol with acetic acid, it was found that accessibility, strength, and nature of acid sites are the key intrinsic characteristics that determine activity and selectivity of a catalyst in this prospective, but scarcely explored route for the valorization of pyrolysis bio-oils (*Appl. Catal. B 2021*). The higher conversion achieved over nanocrystalline *vs.* conventional MFI zeolites of the same chemical composition denoted the significance of the accessibility of acid centers for activation of large-sized guaiacol and for diffusion of the products of its transformation. In turn, the balanced strength of both protonic and Lewis centers was found to provide high selectivities toward targeted value-added hydroxymethoxyacetophenones (HMAPs, Figure 11, *right*). Specifically, the presence of weak Brønsted and Lewis acid centers that facilitate O-acylation side-reaction was shown to be undesirable, while strong BAS that favor side-reaction of guaiacol demethoxylation were found to be partially deactivated during time-on-stream, leading to increased selectivity toward targeted C- acylation products. Thus, nanocrystalline catalysts possessing active sites of medium strength with an appropriate ratio between protonic and coordinatively unsaturated centers (BAS/LAS = 1.4 – 2.2) are favorable catalysts for the conversion of guaiacol to HMAPs.
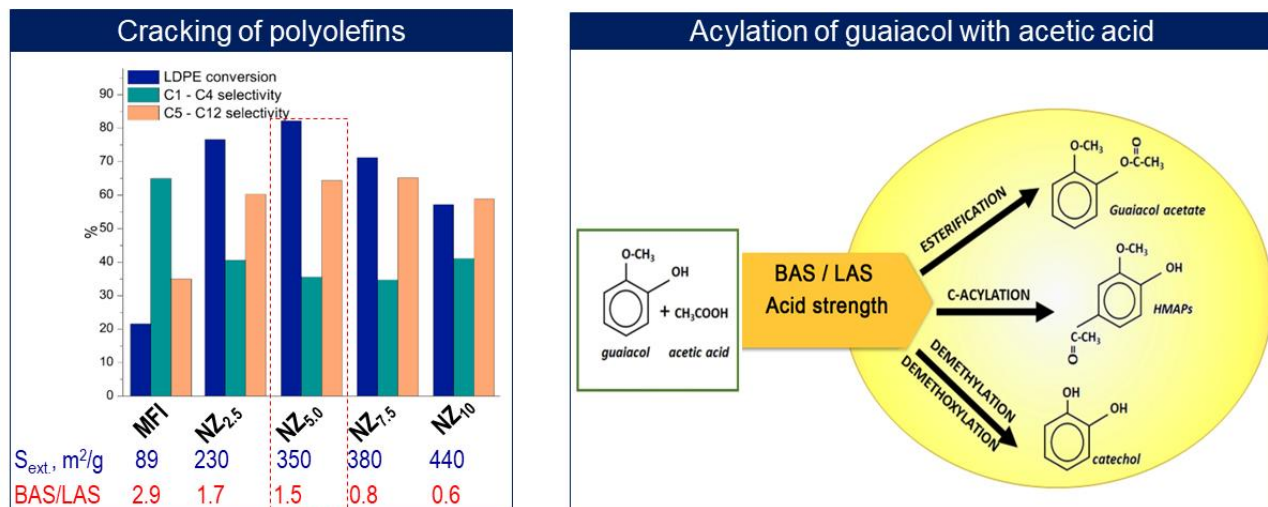
Figure 11. Optimization of the acidic and textural properties of nanocrystalline zeolites for the catalytic cracking of polyolefins (*left*) and guaiacol acylation by acetic acid (*right*). Reprinted from *Micropor. Mesopor. Mater. 2020* and *Appl. Catal. B 2021.*

Layered (2D) zeolites with a thickness of approximately 1–3 nm can be prepared by i) traditional direct *bottom-up* synthesis, as reported for the first documented two-dimensional zeolite, MCM-22P (*ACS Catal. 2021*); (ii) polyquaternary ammonium surfactant-assisted synthesis (Figure 10, *bottom*) using specially designed SDA (*ChemCatChem 2014*); and (iii) a *top-down* method utilizing the propensity of selected 3D zeolites for controllable deconstruction with formation of crystalline 2D nanosheets (*Chem. Soc. Rev. 2015*).

Variations in the synthesis conditions, in particular in the ratio between the components in the starting mixtures, allowed us to prepare a set of nanolayered Al- and Ti-containing MWW zeolites (Si/Al in the range 12 – 35; Si/Ti in the range 35 – 62) with different arrangement of the crystalline layers (i.e., MCM-56 composed of disordered MWW zeolite-type monolayers and MCM-36 composed of MWW zeolite-type layers permanently expanded by amorphous silica props) using either hexamethyleneimine-assisted hydrothermal crystallization or post-synthesis swelling/pillaring approach (Figure 12, *top*). MCM-56 and MCM-36 had a significantly higher external surface (200-380 m^2/g) and an increased portion of highly accessible "external" acid sites (78 – 89 %) than MCM-22 (80 m^2/g, 50 %) reflecting the greater interlayer spacing caused by self-pillaring/silica pillaring in nanolayered materials. A decrease in diffusion limitations had a positive effect on the catalytic activity of nanolayered MCM-36 in selective isomerization of α-pinene oxide to campholenic aldehyde (Figure 12, *bottom*). Ti-substituted MCM-36 with mild Lewis acidity showed unprecedented 96 % selectivity toward the desired product at complete consumption of α-pinene (*Catal. Sci. Tech. 2018*). Such an exceptional behavior of Ti-MCM-36 compared to Ti-substituted zeolites of other structural types and to Al-MCM-36 revealed the crucial role of chemical composition and structure of a zeolite on the outcome of the α-pinene oxide isomerization.
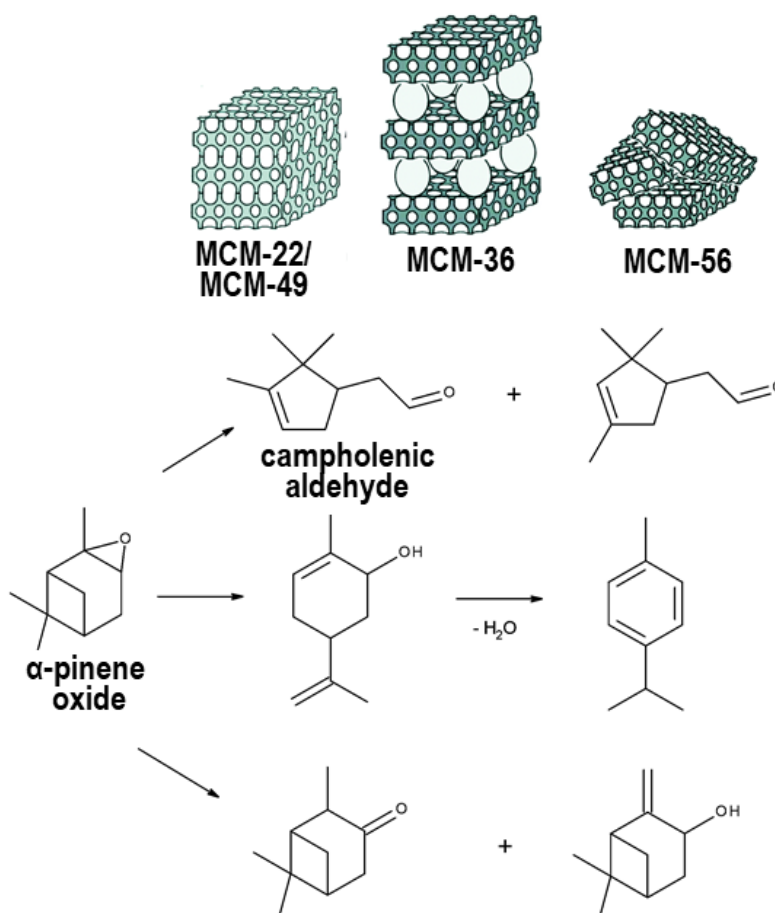
22

Figure 12. (*top*) MWW zeolite family studied in (*bottom*) acid-catalyzed isomerization of α-pinene oxide

Amphiphilic surfactant molecules constructed from polyquaternary ammonium component and long aliphatic chain, which act as templates for zeolite and mesopore-directing agents enabled the preparation of layered MFI catalysts. The use of molecules that have one hydrophobic aliphatic chain, e.g., $C_nH_{2n+1}-N^+Me_2-C_6H_{12}-N^+Me_2-C_6H_{12}$ (n ≥ 16), resulted in the generation of MFI nanolayers with either irregular allocation or ordered arrangement of individual layers. The ordering of the latter structure can be maintained by the introduction of inorganic or organic props covalently bonded to MFI nanosheets (*ACS Catal. 2021*). On the contrary, the use of structure-directing agents with hydrophobic aliphatic chains on both sides of a molecule, e.g., $C_xH_{2x+1}-[N^+Me_2-C_6H_{12}]_y-N^+Me_2-C_xH_{2x+1}$ (x = 18, 22; y = 2; 3; 4) provides thin zeolite nanosheets forming ordered mesostructure (*ChemCatChem 2014*). This approach allowed us to adjust both the wall thickness and the diameters of the mesopores. Variation in the structure of the surfactant molecule (*y* parameter) was used to tune the thickness of zeolite domains in formed materials, while alteration in the size of the hydrophobic aliphatic chain (*x* parameter) was utilized to modify

the size of the mesopores. In our studies (*ChemCatChem 201; ACS Catal. 2015*), we compared the catalytic behavior of 2D zeolites of different morphologies with the performance of traditional zeolites (MFI with 10-ring micropores, BEA with 12-ring micropores, and ultra-stable hierarchical FAU with 12-ring micropores) possessing crystals of micrometer size. Two-dimensional zeolites were represented by materials composed of MFI nanosheets having the same framework Si/Al ratio, diameter of micropores, and quite narrow distribution of mesopores by size. The samples differ only in the thickness of two-dimensional crystalline domains, building the walls of the mesomorphic material, which ranged from 1.7 to 2.7 nm, $M_{1.7-2.7}$ (Figure 13, *left*).
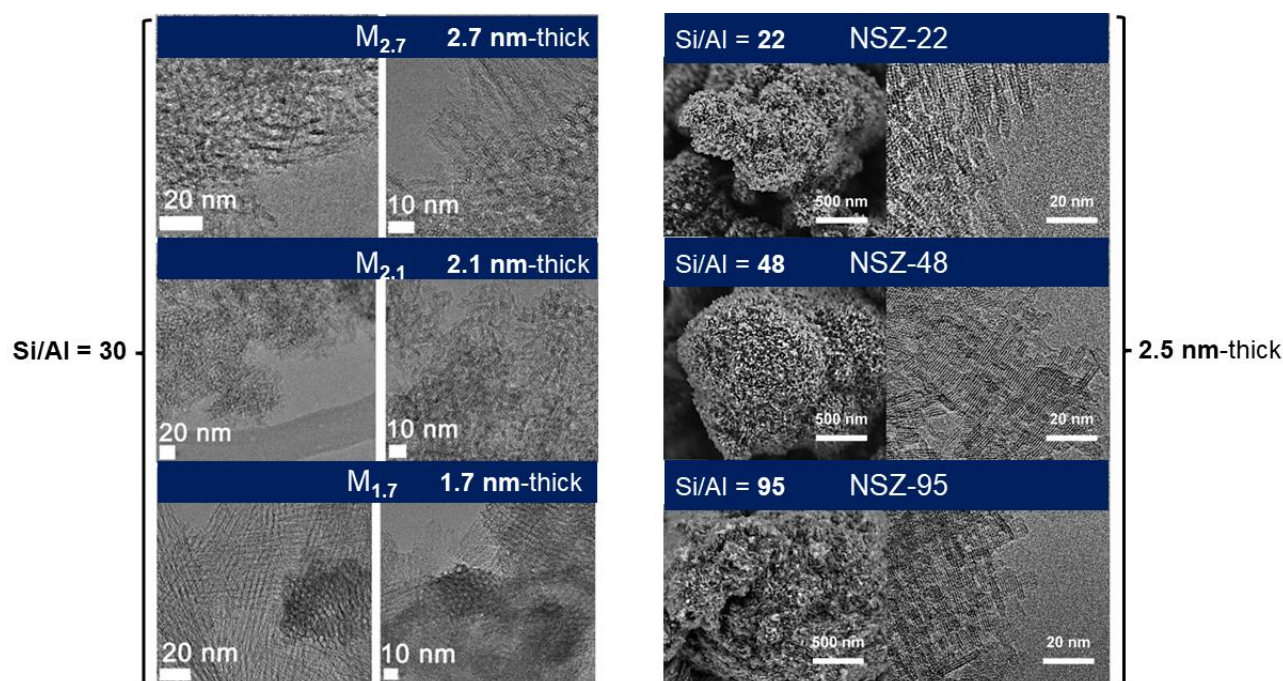

Figure 13. 2D MFI zeolites: (*left*) mesostructured MFI nanolayers, M_n, where n refers to the thickness of the crystalline layers in nm and (*right*) MFI nanosponges, NSZ-x (x refers to the Si/Al ratio in the catalyst). Reprinted from *ChemCatChem 2014* and *ACS Catal. 2015*

Alternatively, 2D MFI zeolites with nanosponge topology were constructed from crystalline nanosheets supporting each other (Figure 13, *right*). The nanosponge MFI were characterized by a Si/Al ratio of 22 (NSZ-22), 48 (NSZ-48), and 95 (NSZ-95). A much higher external surface area was found for all layered materials investigated (Figure 14, *left*). At the same time, 3D zeolites showed a remarkably higher content of acid centers (Figure 14, *right*).
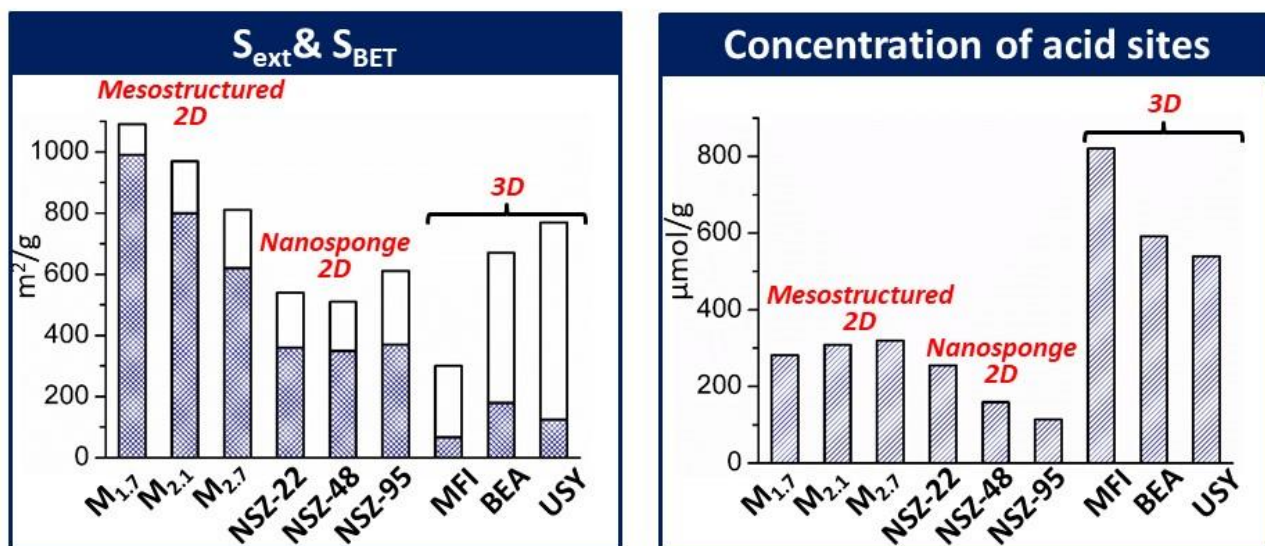
Figure 14. Textural (*left*) and acidic (*right*) characteristics of layered (2D) and conventional (3D) zeolites

In the annulation of phenol with methylbutenol, involving quite small molecules, the yield of desired compounds with the chromane core naturally grows with increasing BET surface area for both 3D and 2D zeolites (Figure 15, *left*). Noticeably, mesostructured two-dimensional zeolites possessing relatively low amounts of acid centers showed higher activity compared to bulk catalysts. The advantageous behavior of two-dimensional zeolites
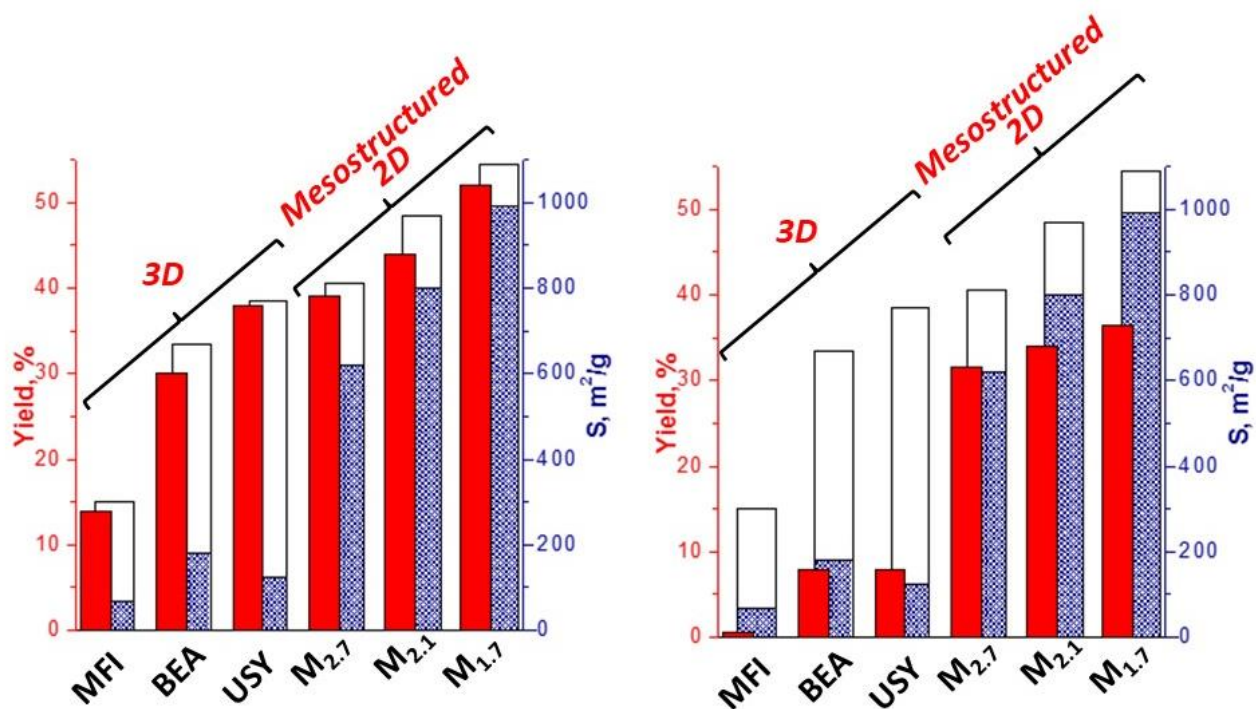

Figure 15. Comparison of chromane yields provided by layered (2D) and conventional (3D) zeolites in annulation of phenol (*left*) and 1-naphthol (*right*)

over conventional catalysts was even more pronounced if bulkier reactant, such as 1-naphthol, was used (Figure 15, *right*). 2D zeolites overcame not just purely microporous MFI and *BEA, but also hierarchical faujasite catalyst. This was related to the optimized diameter of transport channels within the appropriate zeolite mesostructure for the formation of bulky intermediate. The yield of the desired product nicely correlated to the value of the external surface area covered with acid centers accessible for reagents (Figure 15).
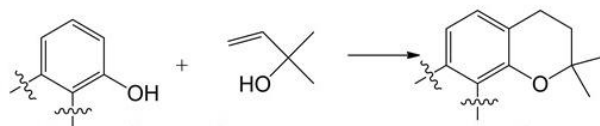
In the condensation reaction of ethyl acetoacetate with pyrogallol, nanosponge zeolites showed higher activity compared to bulk 3D catalysts, which was related to the improved textural characteristics of layered materials. In a range of nanosponge catalysts, the TOF and TON numbers decrease with increasing aluminum concentration, which is usual for zeolite catalysts with close location of Al sites. Nanosponge zeolites were found to be stable and reusable catalysts, maintaining conversion and selectivity values for at least 5 catalytic runs (*ACS Catal. 2015*).
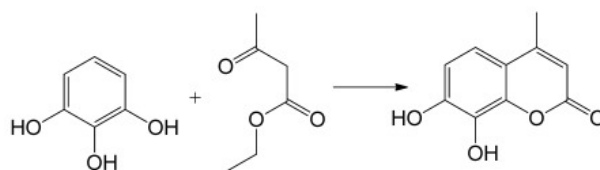
Later on, we applied *operando* infrared spectroscopy to address the activity of 2D and traditional 3D zeolites with MFI structure using model reaction of ethanol-to-DEE dehydration (*Catal. Tod. 2018*; *J. Phys. Chem C 2018*). To get the corresponding values of the first order and zeroth-order rate constants (k_{first} and k_{zero}) and the activation energies (E_{first} and E_{zero}, Figure 16, *top*), the dependence of reaction rate *vs.* ethanol pressure was processed using nonlinear regression. The intensity of the band at 3604 cm^{-1} in the FTIR spectra of the 'working' catalysts was used to estimate the total coverage of Brønsted acid centers and to evaluate the adsorption enthalpies/entropies of ethanol monomeric and dimeric species ($\Delta H_{ads-M \text{ or } D}$, $\Delta S_{ads-M \text{ or } D}$). A lower activation barrier for the bimolecular dehydration pathway, that involves ethanol monomers, was found in layered 2D MFI zeolite (16 kJ/mol) compared to the conventional 3D MFI analogue (41 kJ/mol). In contrast, both catalysts showed similar activation energies for the monomolecular dehydration pathway (117 – 124 kJ/mol), that involves ethanol dimers. Noticeably, the values of the Gibbs free energy of adsorption ΔG_{ads-M} (Figure 16, *bottom*) revealed better stabilization of monomeric alcohol species on 3D MFI in comparison to 2D MFI catalyst. Moreover, less negative value of ΔS_{ads-M} in 2D MFI *vs.* 3D-MFI (-92 ± 10 *vs.* -227 ± 7 J.K^{-1}mol^{-1}) unveiled a lack of confinement for ethanol monomers in layered zeolite. In contrast, ethanol dimers showed similar adsorption entropy in 2D and 3D MFI (-200 ± 13 and -191 ± 10 J.K^{-1}mol^{-1}). Correlating the kinetic parameters of the dehydration reaction with the thermodynamic parameters of ethanol adsorption allowed us to conclude that the difference in the stabilization of various types of adsorbed ethanol species on the catalyst surface was responsible for the difference in catalytic activity of 2D and 3D MFI zeolite studied.
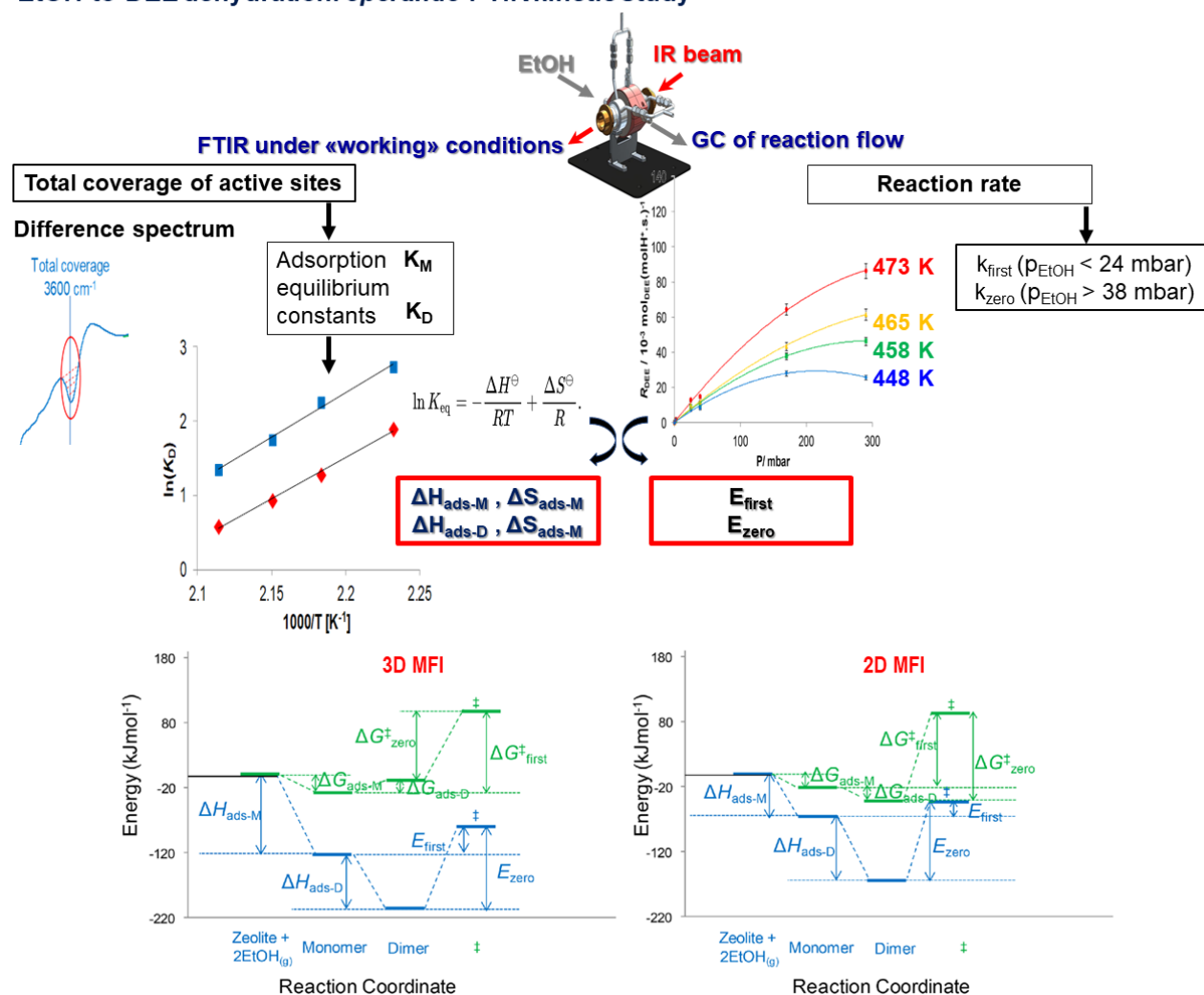
Figure 16. (*top*) Methodology used for kinetic *operando* FTIR study of dehydration of ethanol-to-DEE on 2D and 3D MFI catalysts; (*bottom*) reaction coordinate diagram for ethanol-to-DEE dehydration followed associative mechanism on 3D and 2D MFI zeolites. Reprinted from *J. Phys. Chem. C 2018*

Thus, hierarchical zeolites with highly accessible active centers were shown to be promising catalysts in various acid-catalyzed transformations of different reactants with molecular sizes exceeding the dimensions of zeolite micropore entrances. The decisive characteristics of a hierarchical zeolite catalyst for a specific reaction, such as the strength and nature of the acid sites and the size of the transport pores, can be fine-tuned by optimizing synthesis conditions such as the composition of the reaction mixture and the nature of used organic modifier, among others.

Designing of metal-supported zeolite catalysts

In addition to acid sites, zeolites accept redox active centers by incorporation of metal oxides, transition, and noble metals in their voids. Such metal-supported catalysts are active in the hydrogenation, carbonylation, and selective oxidation of petroleum-derived hydrocarbons. In comparison to unsupported metal species, stabilization of metal nanoparticles (MNPs) on a zeolite support allows one to i) enhance the number of catalytically active surface metal atoms; ii) increase aggregative stability of active phase against sintering; iii) achieve new surface atomic structure-dependent functionalities. Recent research was focused on the influence of the preparation method (Figure 17) and zeolite support characteristics (e.g., structure, chemical composition) on the chemical state and size of metal species to improve their functionality in practical applications.
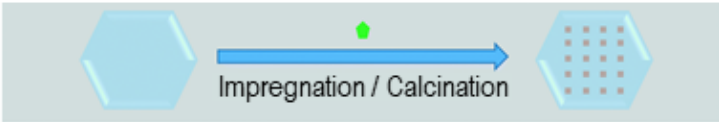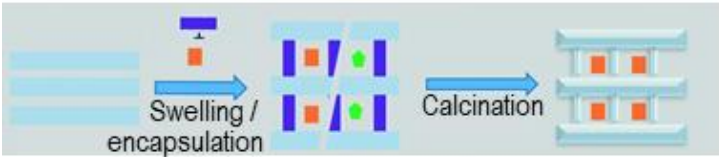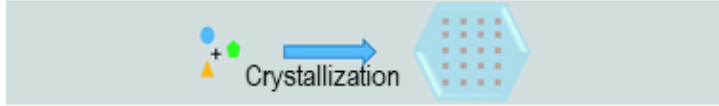
Synthetic strategy used	Advantages	Open questions
Impregnation	-Easy implementation -Low cost	-Effect of the chemical composition of zeolite support on the metal state
2D-to-3D zeolite transformation with metal encapsulation	High aggregative stability and even distribution of metal species within zeolite	Low nominal metal content *vs.* metal loading
In situ encapsulation		Development of stable and "green" protective agents

Figure 17. Methods for the synthesis of metal-supported zeolite catalysts. Adapted from *M. Zaarour et. al, Catal. Sci. Tech., 2020, 10, 8140*

Impregnation is the most common and easy method for the preparation of metal-supported catalysts by soaking a zeolite with a solution of a metal salt of volume equal to the void volume of an activated support (Figure 17, *top*). We have studied the effect of Co loading and the textural and acidic characteristics of the MWW zeolite carrier on the activity of the Co_3O_4-supported catalyst in the oxidation of volatile organic compounds, such as toluene and propane (*ACS Appl. Mater. Interfaces 2021*) The catalysts were prepared by impregnation of zeolite with aqueous cobalt (III) nitrate solutions, followed by calcination at elevated temperature accompanied by the formation of cobalt oxide. The MWW family composed of materials having topologically similar two-dimensional crystalline units with alternating arrangement in the third direction (Figure 12, *top*) and variable aluminum content in the lattice was used to reveal the influence of intrinsic properties of zeolite as a support on the activity of Co-containing materials. Compared to MCM-36 (S_{ext} = 596 m^2/g) and MCM-56 (196 m^2/g) with a well-developed outer surface, MCM-22 (77 m^2/g) provided the highest specific activity among Co_3O_4-based catalysts in both toluene ($TOF_{270\,°C}$ = 3 · 10^{-5} s^{-1}) and propane ($TOF_{215\,°C}$ = 4 × 10^{-5} s^{-1}) oxidation. The superior activity of the MCM-22-supported catalyst was associated with the increased susceptibility of Co_3O_4 to reduction due to

1) the better dispersion of the active oxide phase (as evidenced by STEM);
2) the weaker interactions of metal oxide and the MCM-22 carrier lacking deficient Si–OH groups on the surface (indicated by FTIR spectra showing lower intensities of the corresponding bands in the OH region).

Decrease in the activation barrier for the reduction of Co_3O_4 with decreased Al concentration was exemplified for a set of MCM-22 supports directly prepared with Si/Al = 15 – 50. This effect of the chemical composition of the zeolitic support on the activity of the catalysts was related to (i) the increasing fraction of hardly reducible Co^{2+} located in the ion exchange positions of the zeolites with the decreasing Si/Al ratio in the support (revealed by FTIR using adsorbed pyridine and carbon monoxide); (ii) the decrease in Co_3O_4–zeolite interaction with an increase in Si/Al (indicated by XPS data for Co atoms).

FTIR adsorption studies of reagents allowed us to rationalize different selectivities of Rh-supported catalysts prepared by impregnation of either H- or Na-exchanged form of zeolite BEA in furfural hydrogenation (*Catal. Tod., 2022, 295*). While Rh@H-BEA selectively produced 2-methyl furfural, furfuryl alcohol was selectively obtained on Na-exchanged Rh@Na-BEA catalyst. The FTIR spectra of furfuryl alcohol on Rh@Na-BEA demonstrated weak bands assigned to the non-protonated furfuryl alcohol molecules as the main adsorbed species (Figure 18). In addition to these adsorbed molecules, the formation of the cationic furfuryl alcohol species (corresponding bands appear at 1487 and 1575 cm^{-1}) and diketonic species (1714 and 1621 cm^{-1}) was observed upon interaction of furfuryl alcohol with the BAS of Rh@H-BEA. At temperatures above 350 °C, Na-exchanged Rh@Na-BEA catalyst lost about 75 % of adsorbed furfuryl alcohol species, while most of the species adsorbed in the Rh@H-BEA sample withstood the heating. In this way, Brønsted acid sites ensure strong

interaction with furfuryl alcohol, providing the possibility of its consecutive transformation with formation of 2-methylfuran as the desired product.
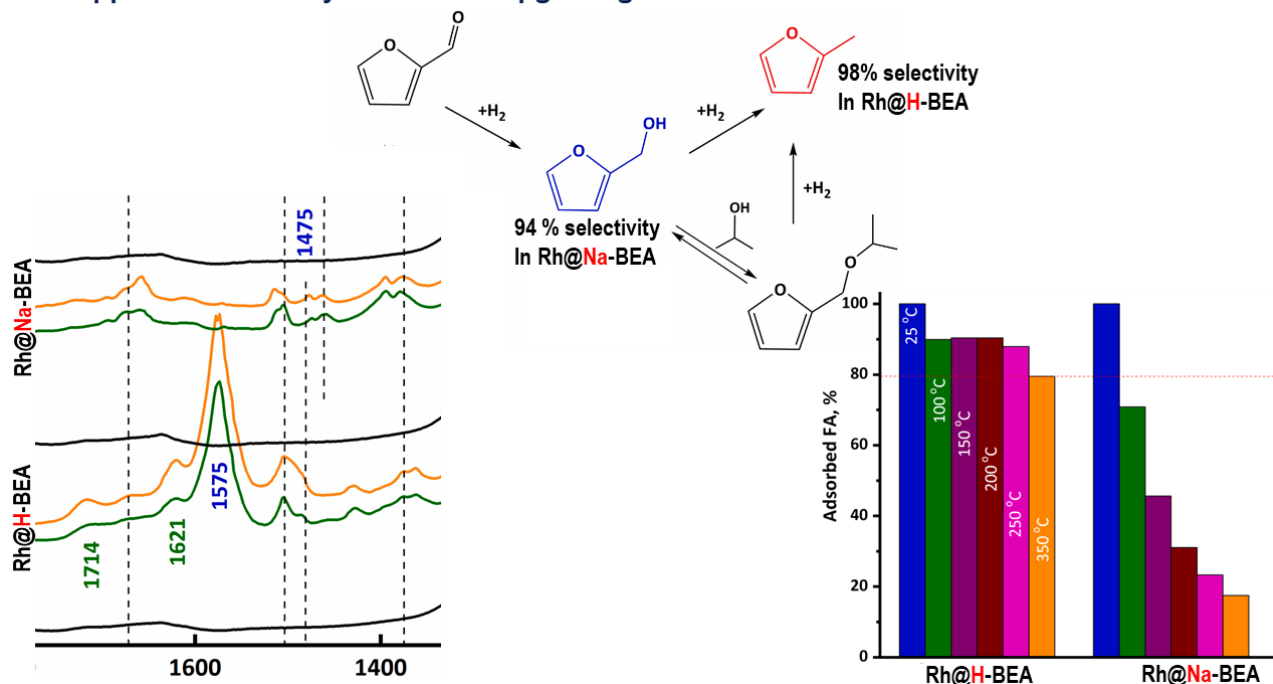

Figure 18. (*top*) Selective hydrogenolysis/hydrogenation of furfural on Rh@BEA zeolites with H$^+$ or Na$^+$ in ion exchange positions. (*bottom, left*) FTIR spectra of catalytic materials activated at 450 °C (**–**), after interaction with furfuryl alcohol, 25 °C (**–**) and 100 °C (**–**) in furfuryl alcohol vibrations region. (*bottom, right*) Change in the intensity of the band at 2939 cm^{-1} upon furfuryl alcohol thermodesorption. Reprinted from *Catal. Tod., 2022, 295*

Although impregnation is the simplest technique for obtaining metal-supported zeolites, this approach suffers from deposition of metal particles on the exterior of the zeolite crystal. Such deposits are characterized by poor dispersion and low aggregative stability, which is a significant disadvantage for the atom-efficient design of costly noble metal-based catalytic materials. A step forward towards maximization of atom efficiency of the preparation method was achieved by (1) combining the transformation process of 2-dimensional (2D) zeolite into 3-dimensional (3D) with introduction of metallic nanoparticles into the internal zeolite voids (Figure 17, *middle*) and (2) *in situ* incorporation of metal component during zeolite crystallization (Figure 17, *bottom*).

2D-to-3D zeolite transformation combined with Pd encapsulation allowed us to benefit from the catalytic activity of Pd MNPs and molecular sieving effect of a zeolite support (*Mater. Tod. Nano 2019*). MCM-22P zeolite layered precursor was swollen with a cetyltrimethylammonium hydroxide solution containing the Pd^{2+}complex, with a subsequent high-temperature treatment aimed at the removal of the swelling agent (Figure 17, *middle*).

STEM images confirmed a high dispersion of Pd (with a mean particle size around ~ 1.8 nm) and the uniformity of its distribution in MCM-22 zeolite (Figure 19). The size of the resulting Pd clusters, apparently larger compared to the micropore size in MWW-type zeolites (0.52 nm), revealed that Pd nanoparticles might occur in the interlayer space limited by adjacent layers that are not fully condensed. Consistently with this assumption, the IR analysis of Pd@MCM-22 featured an absorption band at 3735 cm^{-1} related to the formation of structural defects, internal Si–OH, along with the band of ≡Si-(OH)-Al≡ (3622 cm^{-1}) and external Si-OH groups (3747 cm^{-1}, Figure 19). An additional proof that most metal species were located inside the MCM-22 crystal is a shape-selective behavior of the catalyst in the hydrogenation of nitroarenes to anilines, that is, decent efficiency in reaction involving 3-nitrotoluene as the reactant, while negligible activity when 1-nitronaphthalene was subjected to hydrogenation (Figure 19).
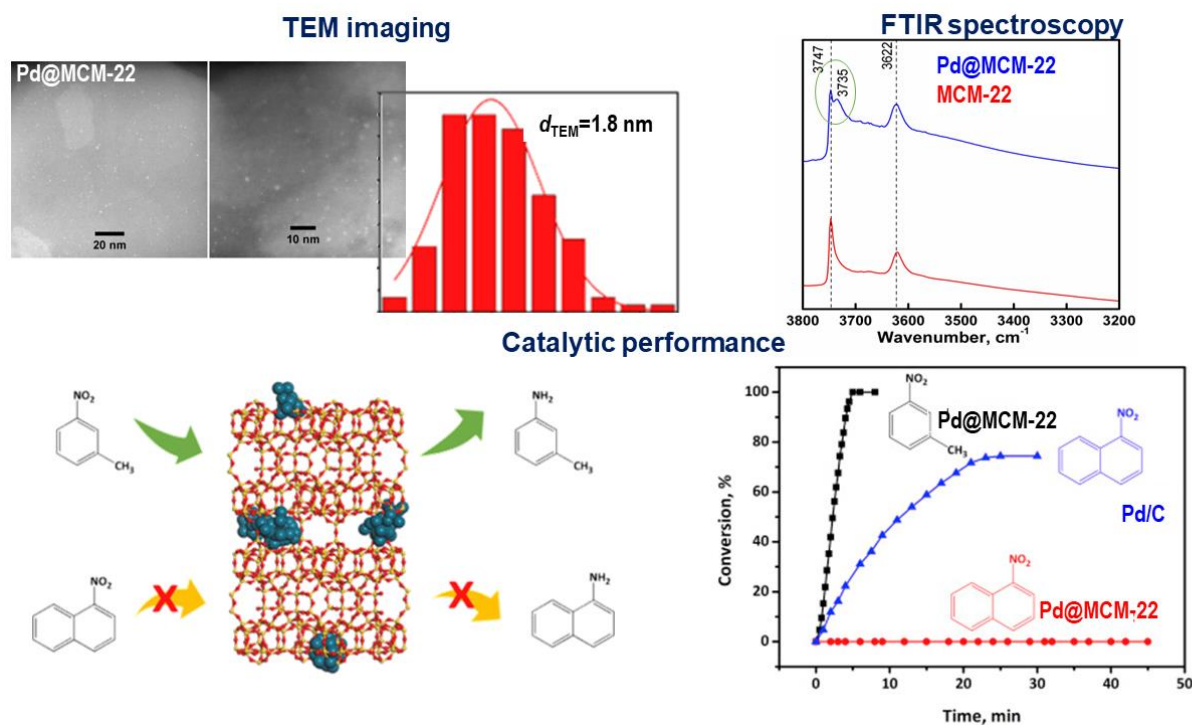

Figure 19. Characteristics of Pd@MCM-22 materials prepared using 2D-to-3D transformation/metal encapsulation. Reprinted from *Mater. Today Nano 2019*

Although 2D-to-3D transformation/metal encapsulation allows the formation of small MNPs in zeolite support and minimization of the sintering/aggregation phenomena, the method leads to Pd@MCM-22 materials with nominal Pd loading (0.79 wt. %) 5-times lower compared to the one used in a synthesis mixture (4 wt.% of zeolite mass). To improve further the atom efficiency of the 2D-to-3D transformation/metal encapsulation approach, we have split the interlayer expansion and metal incorporation stages (*Catal. Tod. 2022, 109*). The nominal Pd loading in the thus prepared Pd@MCM-22 catalysts corresponded to the one determined in a material by chemical analysis, while its catalytic activity (i.e., the Pd weight-

normalized initial reaction rate) in the 3-nitrotoluene-to-3-aminotoluene hydrogenation twice exceeded that for the catalyst prepared by the unmodified approach and containing larger Pd species.

Alternatively to the post-synthesis method of 2D-to-3D zeolite transformation / metal encapsulation, the *in-situ* **approach** (Figure 17, *bottom*) for the preparation of metal-supported zeolite catalysts relies on the crystallization of zeolites in the presence of metal precursors. This synthetic approach uses N- and S-containing protective agents, such as organic amines and mercaptosilanes, to prevent fast precipitation and segregation of bulk metal hydroxides under harsh conditions (elevated temperature, alkaline medium). We first used 1-methyl-3-(triethoxysilyl propyl) as environmentally friendly imidazolium-type ionic liquid (ImIL) for the *in-situ* preparation of Pt- and Pd-supported MFI zeolites (*Chem. Eng. J. 2021*). For that, 1-methylimidazole known as the structure-directing agent for zeolite synthesis was functionalized with triethoxysilyl propyl groups, thus providing (i) positively charged imidazolium groups, which can stabilize metal precursors or small metal nanoparticles, and (ii) the alkoxysilane parts that take part in the crystallization of MFI zeolite (Figure 20).
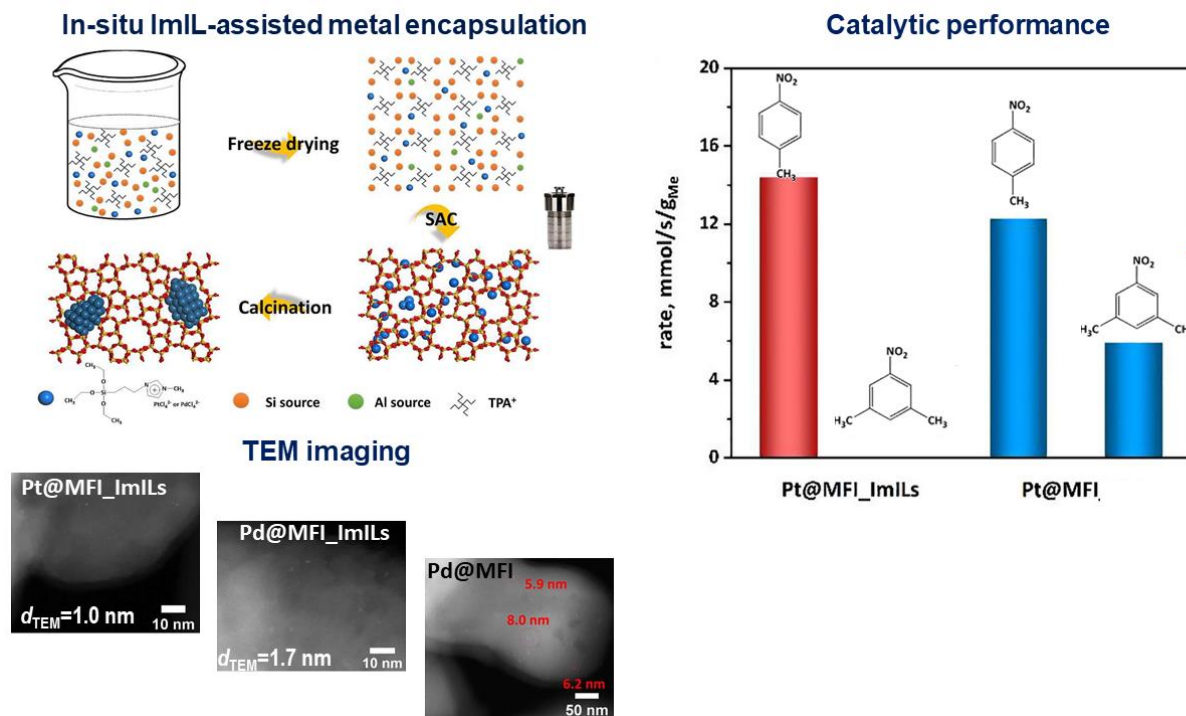

Figure 20. *In situ* ImIL-assisted metal encapsulation for the preparation of Pt@ and Pd@MFI_ImILs catalysts and their characteristics *vs.* Pt@ and Pd@MFI prepared using impregnation method. Reprinted from *Chem. Eng. J. 2021*

The STEM images and EDS maps of thus prepared Pt@MFI_ImILs and Pd@MFI_ImILs catalysts confirmed the uniform distribution of Pt and Pd within a support with the mean size

of MNPs around 1.0 and 1.7 nm, respectively. On the contrary, the Pt@MFI and Pd@MFI samples prepared by the traditional impregnation method form larger MNPs (> 6 nm), mostly located on the outer surface of the zeolite crystals. The efficient encapsulation of MNPs into zeolite matrix upon ImILs-assisted crystallization was reflected in shape selective hydrogenation of nitroarenes: hydrogenation of small 4-nitrotoluene to 4-aminotoluene occurred over both Pt@MFI_ImILs and Pt@MFI, while bulky 1,3-dimethyl-5-nitrobenzene was hydrogenated on Pt@MFI containing Pt nanoparticles on the external surface, but not over Pt@MFI_ImILs. The result is related to a larger kinetic diameter of 1,3-dimethyl-5-nitrobenzene compared to the pore size of MFI zeolite, preventing diffusion of the reactant to the encapsulated Pt species.

Thus, our recent achievements in the synthesis of nanomaterials enabled a more precise control over the type and size of the supported metal nanoparticles at the catalyst preparation stage. The most critical factor determining the catalytic performance of MNPs, their size, was minimized using the emerged methods of 2D-to-3D zeolite transformation with metal encapsulation and in situ metal encapsulation.

Conclusions and outlook

The presented studies on tailoring the "nanoscale" characteristics of active sites in zeolites, such as their nature, amount, and accessibility combined

(i)   the development of synthetic methods for zeolite catalysts with unusual structures and compositions

with

(ii)   spectroscopic studies of their catalytic chemistry to understand the processes at the molecular level.

As a result, advanced catalysts with properties that are far more interesting than those of conventional materials became feasible. Despite these advances, the designed catalysts contained myriads of structurally dissimilar active sites, because the "atomic-scale" engineering of the zeolites remained beyond the scope of the synthetic methods developed.

However, our progress in the chemoselective manipulation of germanosilicate zeolite frameworks may provide the basis for solving one of the longstanding key challenges in material design, atomic-level engineering of reactive ensembles within heterogeneous catalysts to create a new class of single-site zeolite acid catalysts. Such materials must advance the mechanistic description of heterogeneous catalysts at the atomic level by promoting thorough experimental and computational studies on structure-function relationships, wherein a given function is analyzed across a wide range of possible atomic-level configurations of metal active sites. Establishment of a synthetic method for atomic-scale engineering of key features of zeolite acid sites would change the experimental paradigm in zeolite research from the current trial-and-error strategy to predictive engineering of target catalytic functions.